TRANSPORT PHENOMENA
IN SUBLIMATION DEHYDRATION

A THESIS

Presented to

The Faculty of the Graduate Division

by

David F. Dyer

In Partial Fulfillment

of the Requirements for the Degree

Doctor of Philosophy

in the School of Mechanical Engineering

Georgia Institute of Technology

September, 1965

In presenting the dissertation as a partial fulfillment of the requirements for an advanced degree from the Georgia Institute of Technology, I agree that the Library of the Institution shall make it available for inspection and circulation in accordance with its regulations governing materials of this type. I agree that permission to copy from, or to publish from, this dissertation may be granted by the professor under whose direction it was written, or, in his absence, by the Dean of the Graduate Division when such copying or publication is solely for scholarly purposes and does not involve potential financial gain. It is understood that any copying from, or publication of, this dissertation which involves potential financial gain will not be allowed without written permission.

_____

_____

TRANSPORT PHENOMENA

IN SUBLIMATION DEHYDRATION

Approved:

Chairman

Date approved by Chairman August 25, 1965

ACKNOWLEDGMENTS

The author is grateful to many people who through the previous years have encouraged and aided him in his educational work. An expression of appreciation is due several men who have helped him in his graduate work.

First, a special note of thanks is due Dr. J. E. Sunderland who serving as my advisor offered sage counsel and enthusiastic encouragement in this investigation and throughout the period of graduate study. He is to be especially commended for the personal interest which he manifests in his students. The constructive comments and time given by the thesis committee, Dr. Henry McGee and Dr. Thomas W. Jackson are gratefully acknowledged. Also the author is deeply appreciative of the assistance given by Mr. C. R. Bannister in the fabrication of the experimental apparatus. Also a note of thanks is due the author's brother, Richard, who helped in the experimental investigation.

The author would like to thank his parents, Mr. and Mrs. J. M. Dyer, Sr. for their guidance and encouragement during his early life and for the home environment which has helped him through his educational endeavor. Sincere appreciation goes to his wife, Angie, whose unceasing love and devotion have greatly assisted him.

The author wishes to express his gratitude to the United States Department of Health, Education, and Welfare for a NDEA fellowship to support his graduate studies and for Public Health Research Grant EF 00102-02 from the Division of Environmental Food Protection which

provided partial support for this investigation.

Finally, the author is supremely grateful to God for the extension of unmerited physical, mental, and spiritual blessings throughout his life.

TABLE OF CONTENTS

LIST OF TABLES

LIST OF ILLUSTRATIONS

SUMMARY

Experimental and analytical studies are presented for freeze-drying of beef. To predict freeze-drying rates analytically, accurate data on permeability and diffusion coefficients for air water-vapor transport through freeze-dried beef are essential. Previous to this investigation, no experimental data for diffusion coefficients for flow through freeze-dried beef existed. The permeability data for beef presented in the literature vary as much as 1000 per cent. One of the boundary conditions used in analytically determining drying rates involves the relationship between the equilibrium partial pressure and temperature for the food product. No experimental data giving this relationship existed before this investigation. In addition, the analytical equations for prediction of drying rates available previous to this investigation do not properly describe the mass transport under conditions of combined bulk and diffusional transport. Therefore, the objective of this paper is to determine experimentally and, as much as possible, theoretically the following properties: permeability, diffusion coefficient, and equilibrium vapor pressure. Using these property values it is desired to develop a mathematical model which accounts for and shows the entire mechanism of heat and mass transport in freeze-drying and to obtain a closed form solution for the equations resulting from the mathematical model. From these equations optimum conditions for freeze-drying are to be inferred. This objective is carried out by first conducting experimental and theoretical investigations of the three

properties desired. Analyses are then made for a variety of assumptions and boundary conditions using the property values obtained in the initial part of the investigation.

Starting from a basic force balance the equation of motion for the flow of a gas or gas mixture through a tube is developed. Non-continuum effects are accounted for in the derivation. Using the conventional definition of permeability and the derived equation of motion, a permeability for non-continuum transport in a capillary is derived in terms of the pressure drop across the capillary, the average gas pressure and temperature, and capillary geometry. This equation is modified for flow through the porous freeze-dried meat and allows the determination of the effect of temperature on permeability. An experimental investigation using two different methods was conducted for determination of the permeability. The experimental results for permeability were found to have a 10 per cent deviation due to sample variations and also to be thickness dependent. The initial theoretical work did not predict this effect. A postulate account for the thickness dependence is made that the capillaries are crimped at the ends and this postulate is verified using the experimental data. The experimental data cover a pressure range of approximately .5 to 4 torr and sample thicknesses from .0625 to .125 feet. The samples used were taken from different cuts of beef and were frozen initially at several rates.

An experimental study of the equilibrium vapor pressure of frozen bovine muscle is presented for a temperature range of -23 °C to -1 °C. Measurements are presented for round, sirloin, and T-bone steak. The results show that the equilibrium vapor pressure of beef is approximately

20 per cent lower than the vapor pressure of pure ice at the same temperature. An interpretation of the experiments attributes the vapor pressure depression to dissolved solute species in the frozen liquid phase of the beef muscle. To determine the role of the solid meat matrix in the vapor pressure depression, experimental measurements are also presented for the vapor pressure of the frozen liquid phase which can be mechanically removed from the meat by squeezing at room temperature. The vapor pressure of this phase at a given temperature lies between that of beef muscle and pure ice. This result is interpreted by use of a simple model which idealizes the beef muscle as a cross-linked ionic network which contains not only soluble and mobile ionic species, but also ions and other hydrophilic groups which are permanently attached to the network. Due to the presence of these permanently attached groups, more solute particles are present in the frozen liquid phase when it is incorporated in the meat matrix than is the case when it is removed. Since the magnitude of the vapor pressure depression increases with the concentration of dissolved solute species, the depression is greater when the meat matrix is present. These ideas are consistent with the observed temperature coefficient of the vapor pressure, which is larger for frozen beef muscle than for the separate frozen liquid phase.

Analytical and experimental analyses are presented for bulk and diffusional flow of a binary gas mixture under steady-state conditions. The analysies are valid for the entire region between pure molecular and viscous flow. The analytical analysis is made for flow through a capillary tube subjected to a small pressure gradient. A momentum balance is applied to one component of the gaseous mixture in order to

determine an equation for the rate of transport of that component.

Analytical results for the capillary tube are modified for the case of transport through a porous material by considering this material to be a bundle of capillary tubes. Experimental results for the effective average diffusion coefficient for the transport of an air water-vapor mixture through freeze-dried meat are presented; these results compare favorably with the analytical results for the porous material.

Thermal transpiration effects are considered by some investigators to be important. In order to decide if this factor is indeed significant in the analytical work an experimental and theoretical investigation into thermal transpiration in freeze-drying is made. Both the theoretical and experimental findings indicate that the order of this effect is less than 3 per cent.

The first analytical solution presented is "exact" in that it encompasses time variations in properties as well as space changes. In order to obtain a closed form solution fixed boundary conditions at the surfaces and interface of the food product are used and no heat input to the interface from the frozen region is considered. These boundary conditions uncouple the mass and energy transfer equations and allow a separate solution of the equations; thus, the solution becomes much simpler. Secondly a similar "quasi-steady" solution is given differing from the first in that the time rates of change in properties are assumed negligible in comparison to space the rate of change. Comparison of the two solutions shows that the quasi-steady solution is accurate within approximately 2 per cent.

Experiments by other investigators show that the interface temperature does not remain constant during drying. Consequently, a third

solution is presented in which the mass and heat transfer equations are coupled (i.e., solved together). The "quasi-steady" assumption is made since the assumption is shown to be good by comparison of the first two solutions. The boundary conditions for this solution are all directly controllable external conditions, namely the temperature, total pressure, and water-vapor partial pressure at the heated surface and the temperature of the face opposite to the heated face. This solution clearly shows the mechanisms involved in freeze-drying and allows the accurate determination of the interface position and temperature. This solution shows that the interface temperature is constant only when there is no heat input to the interface through the frozen region. For the non-adiabatic case at high chamber concentrations of water-vapor, the interface temperature is shown to approach closely the equilibrium temperature for meat at the chamber pressure. Since it is assumed in the first two solutions that the interface temperature corresponds to the equilibrium temperature for the chamber pressure, the solutions are very closely correct at high chamber water-vapor concentrations.

Comparison of the results for the first two solutions and the third solution show that the first two solutions give a relatively good approximation to the more refined third solution. However, they do not afford a good insight into the mechanisms of freeze-drying.

Of special interest is the role of mutual diffusion with respect to hydrodynamic flow in freeze-drying. Typical results are calculated using the third solution and show that the diffusional flow contributes about 50 per cent as much as the hydrodynamic transport.

The third solution shows that faster drying is achieved by

decreasing the chamber pressure, decreasing the chamber partial pressure and heating from the back face. The first two effects are seen to cause only small variations in drying time with pressure while the third effect tremendously reduces the drying time.

NOMENCLATURE

Symbol		Typical Units
a	molar flux factor, $1 + N_2/N_1$	dimensionless
A	area	ft^2
b	proportionality constant defined on page 89.	$ft/(sec)^{1/2}$
b_3	coeffieient defined by $b_4C_9 8SRT/3\pi aD_{k2}$	lbf/ft^2
b_4	coefficient defined by $-N_2aL/C_9$	dimensionless
B	term defined on page 16	B/sec ft
B_3	coefficient defined on page 100	ft^3/lbm sec
B_4	coefficient defined on page 99	ft^2
B_5	coefficient defined on page 99	lbf/ft^2
$C1, C2, C_3, \ldots, C_8$	integration constants	
C_9	constant defined on page 24	mole/ft-sec
$C_{10}, \ldots, C_{14}$	integration constants	
C_{15}	constant defined on page 33	mole/ft-sec
C_F	force coefficient defined on page 96	lbf sec/ft^3
C_p	specific heat	B/lbm °R
$\tilde{C}_p$	molar specific heat	B/mole °R
D	mutual diffusion coefficient	ft^2/sec
D_K	Knudsen's diffusion coefficient defined by $(2/3)r_c\bar{V}$	ft^2/sec
F	external force	lbf
$F(r_c/\lambda)$	fraction of molecules not undergoing intermolecular collisions	

Symbol		Typical Units
ΔH	heat of sublimation $(\Delta\tilde{H})/M$	B/lbm
$\Delta\tilde{H}$	molar heat of sublimation defined on page 99	B/mole
k	thermal conductivity	B/ft sec °R
k_{eI}	effective thermal conductivity of region I defined on page 87	B/ft sec °R
K	Boltzmann's Constant	B/molecule °R
$K(p_m,\Delta p)$	reduction of mass flow due to capillary "crimping"	lbm/ft^2 sec
Kn	Knudsen number	dimensionless
L	sample thickness	ft
m	mass of molecule	lbm
M	molecule weight	lbm/lbm-mole
n	molecular concentration	$molecules/ft^3$
N	molar flow rate	$moles/ft^2$ sec
p	total pressure	lbf/ft^2
$\bar{p}$	partial pressure	lbf/ft^2
Δp	differential pressure defined by $p_L - p_o$	lbf/ft^2
r	radius	ft
r_c	capillary radius	ft
R	gas constant	ft-lbf/lbm °R
$\tilde{R}$	universal gas constant	ft-lbf/mole °R
S	reflection coefficient defined by fraction of incoming molecules which are reflected diffusely	
t	time	sec

Symbol		Typical Units
T	temperature	^{o}R
T(x,t)	temperature evaluated at position x and time t	^{o}R
u	macroscopic gas velocity	ft/sec
U	coefficient defined on page 11	
$\bar{V}$	average molecular velocity defined on page 23	ft/sec
W	mass flow rate	$lbm/ft^2 sec$
W'	mass flow rate accounting for crimping effect at end of capillaries	lbm/ft^2 sec
x	axial tube coordinate	ft
X	position of interface between region I and II	ft
y	molar concentration	$\frac{\text{moles of component}}{\text{moles of mixture}}$
z	non-dimensional axial distance defined by x/L	dimensionless

Greek Symbols

α	thermal diffusivity	ft^2/sec
α_{eI}	effective thermal diffusivity of Region I defined on page 87	ft^2/sec
γ	term defined on page 16	B/sec
Γ	first order correction introduced on page 99	
ε'	permeability defined on page 64	ft^2
ε'_L	partial derivative of ε' with respect to L for constant mean pressure and temperature	ft
$\tilde{\varepsilon}$	molar permeability defined on page 64	ft mole/lbf sec
$\varepsilon(p_m)$	permeability defined on page 101	ft^2

Symbol		Typical Units
η	parameter defined on page 10	
θ_I	non-dimensional temperature defined on page 10	dimensionless
θ_{II}	non-dimensional temperature defined on page 15	dimensionless
$\theta_I(x,t)$	θ_I evaluated at position x and time t	dimensionless
$\theta_{II}(x,t)$	θ_{II} evaluated at position x and time t	
λ	mean free path	ft
μ	viscosity	lbm/ft sec
ν	coefficient defined on page 89	dimensionless
$\bar{\nu}$	coefficient defined on page 90	sec/ft^2
ρ	density	lbm/ft^3
$\tilde{\rho}$	molar density	$mole/ft^3$
σ	porosity	dimensionless
τ	tortuosity factor	dimensionless
Φ	parameter defined on page 82	dimensionless
ω	quantity defined on page 9	B/ft^3

Subscripts

a	air
c	at capillary surface
D	dried layer
e	effective value
i	ice
L	at capillary exit
m	average value

Symbol

M	mixture
t	transition regime
v	vapor
X	position of interface
w	water-vapor
0	capillary entrance
1	component 1
I	region I
II	region II
2	component 2

CHAPTER I

INTRODUCTION AND HISTORICAL BACKGROUND

Freeze-Drying

The freeze-drying process involves the following basic operations: The food product is frozen and then placed in a vacuum chamber which is evacuated to a pressure lower than the ice triple point. Heat is applied to the product and because the operation is carried out below the ice triple point, the water substance* in the product sublimates. A typical laboratory freeze-dryer, which illustrates the essential features of the commercial apparatus, is shown schematically in Figure 1. Harper and Tappel (1)** give an excellent detailed description of the development and operation of commercial equipment for freeze-drying.

Several advantages ensue from this method of food processing; for example, the food product can be stored at room temperature up to a year, handling is simplified since the weight loss ranges up to 80 per cent, little shrinkage results, and the taste and nutritional quality are retained.

Historical Development and Related Literature

Most of the literature concerning freeze-drying deals with the biological aspects of the process. A complete summary of these aspects is considered in a book edited by Harris (2). An especially

*The liquid in meat is essentially water but contains salts and other dissolved substances.

**Numbers within parentheses refer to items listed in the Bibliography.

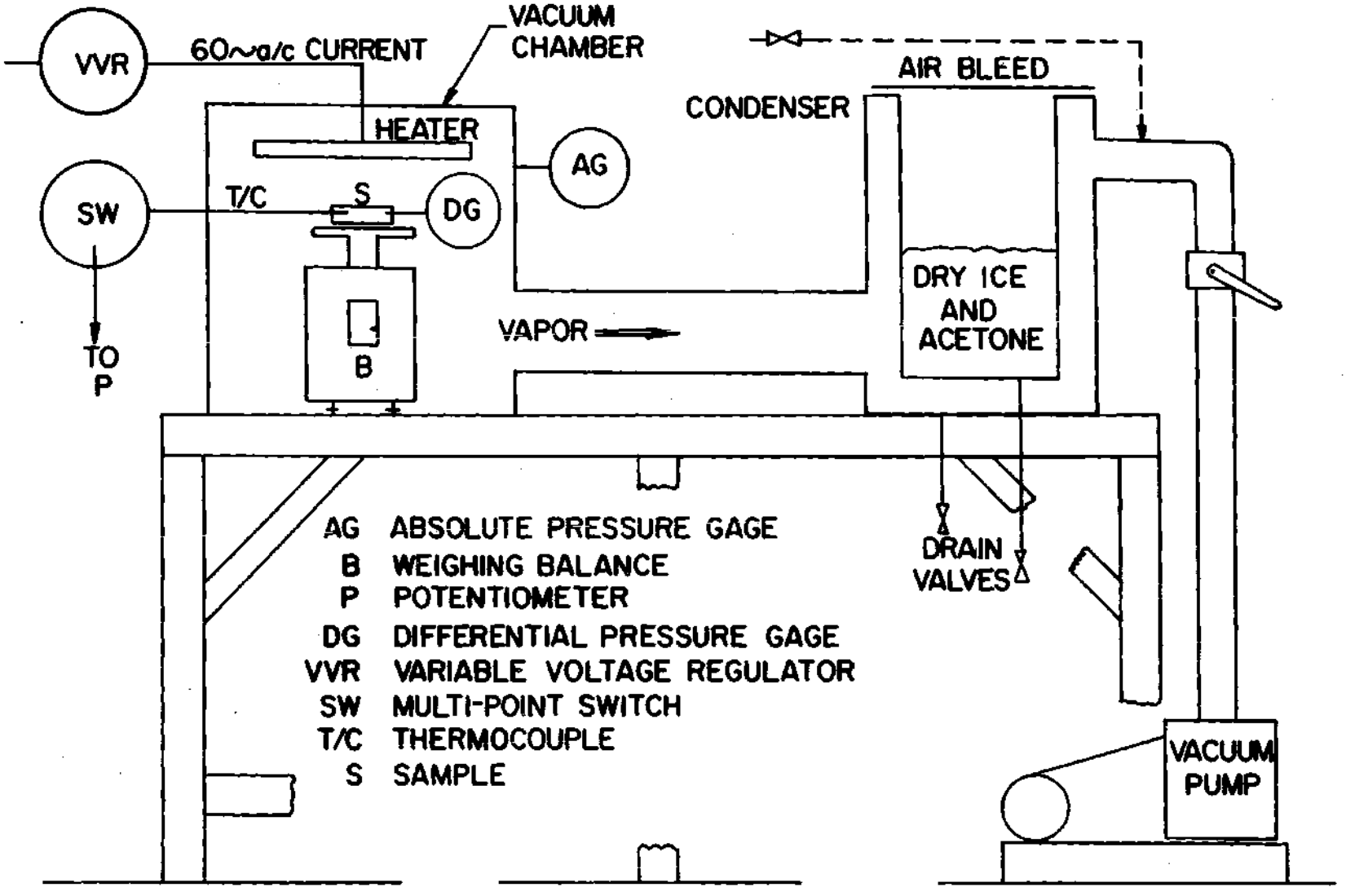

Figure 1. Typical Laboratory Freeze-Dryer.

important reference of the physio-biological properties of freeze-dried products is presented in the work by Luyet (3).

A summary of the analytical work directly related to this problem which has been presented in the literature is as follows:

(a) Flosdorf's (4) book written in 1949, which is the result of his experience with laboratory and commercial freeze-drying apparatus, presents an analytical treatment which is outdated (for example adiabatic flow was assumed). However, he presents an excellent historical review of freeze-drying developments before 1949.

(b) Lambert (5) in 1956 analyzed the freeze-drying process in the same manner as heat transfer through a composite wall (i.e., as several resistances in series). He determined overall coefficients but his analysis does not clearly show what the heat and mass transfer mechanisms are.

(c) Harper and Tappel (1) presented an analytical investigation in 1957 which provides a basis for an accurate analysis, but they make several strong simplifying assumptions; isothermal flow, drying rate independent of energy input, and constant properties. Also they do not combine their diffusional flow with the hydrodynamic flow. The main conclusion of their work is that the drying time is proportional to the square of the thickness of the food sample.

(d) In 1961 Bannister (6) and in 1963 Koumoutsos and Sunderland (7) presented similar analyses on the basis of flow through a bundle of capillaries and account for slip effects with kinetic theory. Their diffusion equation is only applicable to the case of constant total pressure which does not correspond to the usual situation. They solve

the heat transfer coupled with the mass transfer equations with several simplifying assumptions for the various flow regimes but indicate that additional work is needed to clarify when the various effects must be accounted for. Their chief result coincides with that of Harper and Tappel.

Several publications not directly related to the analytical work on the freeze-drying process but which are important to an understanding of the various mechanisms involved are: Kennard's (8) and Loeb's (9) discussion of slip and free molecular flow, Carmen's (10) discussion of the application of Kennard's equations for flow in a porous media, Schneider's (11) work on conduction and convection heat transfer through porous media, Bird, et al., (12) analysis of diffusive mass transfer, and Scott and Dullien's (13) and (14) discussion of diffusive and bulk flow in the transition region.

Important experimental measurements are presented by Harper (15) and (16) and by Harper and Tappel (6). All of these references contain essentially the same data. While important, these data on permeability and diffusional resistance, by the author's admission, are subject to considerable experimental error. These works present permeabilities for a few samples for several pressures. Also values of porosity and the ratio of free diffusion to diffusion through the dried sample are given. In addition, Harper and Chichester (17) present new but conflicting data with that of these earlier publications.

Hardin (18) presents important experimental data for temperature and pressure distributions and drying rate for beef for a range of chamber pressures and concentrations. Also he presents analytical work

for prediction of the experimentally observed data. He was not concerned with obtaining property data for the beef and his analytical work is applicable only for quasi-steady drying for which mutural diffusion can be neglected. He presents an excellent detailed description of the important literature concerning experimental and analytical work in freeze-drying as well as the historical development of the process.

Purpose and Scope

The great disadvantage to freeze-drying is the large amount of time required to dry the product. Due to the scarcity of accurate property data and the lack of data in some areas as indicated by the above review, it has been impossible to carry out analytical studies for optimizing the drying rate. Futhermore, it is seen in the previous literature, due partly to a lack of understanding of the freeze-drying process, that the analytical work needs considerable refinement.

Since it is quite desirable to greatly increase freeze-drying rates, one purpose of this work is to determine properties and analytical results for predicting optimum conditions for freeze-drying of beef steak. As a consequence of the deficiencies pointed out above, it will be necessary to conduct tests on freeze-dried beef steak checking the previously determined property data and obtaining new data in areas not already studied. The previously mentioned analytical work is to be extended and refined. It will be used in conjunction with the property data for showing the effect of the important parameters on freeze-drying.

The scope of the property data measurements will include the determination of permeability coefficients (see page 101) and average

diffusion coefficients (see page 25) for different grades and cuts of freeze-dried beef steak frozen and dried under different conditions. The measurements will be made under the conditions normally encountered in freeze-drying work. The thermal conductivity is also needed, but this property is being studied separately by Hill (19) and Massey (20). In addition to this work, the vapor pressure of frozen beef will be determined.

The scope of the analytical work will include the analytical determination of the drying time for the freeze-drying of beef with appropriate boundary conditions. Assumptions necessary for obtaining a closed form solution will be made and a check of the error introduced by the assumptions will be made where possible.

CHAPTER II

ANALYTICAL INVESTICATION OF UNCOUPLED MASS AND HEAT TRANSFER IN FREEZE-DRYING

Mathematical Statement of the Problem

During freeze-drying of solid food products, it has been found that the grain orientation has considerable influence on the direction that the vapor moves through the drying solid. Consequently, the pore structure of the dried food product is such that there is a complex path in one general direction which can be idealized as a tortuous bundle of capillary tubes of non-uniform cross section. As drying proceeds, a dried layer forms on the heated side and is distinctly separated from the frozen layer of the product. The interface thickness between the dried and frozen layer has been measured by Hatcher (21) and found to be less than 5 mm thick. The vapor flows from this interface through the complex path offered by the dry layer. For mathematical analysis the interface will be assumed to be perpendicular to the vapor flux direction (i.e., to the general capillary or grain direction) and to move parallel to itself. In order to achieve this condition experimentally, the heat flux must be in the opposite direction to the vapor flow and the free surface must be perpendicular to the grain direction. Heat is generally radiated to the free surface by a radiant heater.

Two general cases will be considered analytically in this chapter. Non-steady drying will be considered in case 1; but in the boundary

condition which relates the heat input at the interface and the mass flow rate, the heat storage in the dried layer is neglected. This assumption is quite valid since calculations by the author based on typical experimental data by Hardin (18) show that the heat storage to the dried layer represents less than one per cent of the total energy input. In case 2 the "quasi-steady" model is used in which the time rate of temperature change in the governing energy equations is considered negligible in comparison to the space rate of change.

It is desired to determine expressions for the temperature distribution and drying rate for the two cases outlined above. The boundary conditions are to be chosen such that the heat and mass transfer equations are independent.

Governing Equations

For convenience the dried and frozen layers will be designated by Region I and Region II respectively. By making an energy balance on Regions I and II, the equations appearing below are derived (see Appendix A):

For Case I, Region I

$$\frac{\partial T_I}{\partial t} - v \frac{b}{2\sqrt{t}} \frac{\partial T_I}{\partial x} = \alpha_{eI} \frac{\partial^2 T_I}{\partial x^2} \tag{2.1}$$

For Case 1, Region II

$$\alpha_{II} \frac{\partial T_{II}}{\partial x^2} = \frac{\partial T_{II}}{\partial t} \tag{2.2}$$

For Case 2, Region I

$$\frac{d^2T_I}{dx^2} + \bar{v}_I \frac{dX}{dt}\frac{dT_I}{dx} = 0 \tag{2.3}$$

For Case 2, Region II

$$\frac{d^2T_{II}}{dx^2} = 0 \tag{2.4}$$

Boundary Conditions for Case 1

For Region I

Hatcher (21) showed that the interface temperature remains nearly constant for drying with a constant chamber pressure greater than 0.5 torr and approximately equal heat input from both sides of the meat. These conditions along with an energy balance at the interface and the initial location of the interface form the set of boundary conditions:

$$T_I(0,t) = T_0 \tag{2.5}$$

$$T_I(X,t) = T_X \tag{2.6}$$

$$K_{II}\left.\frac{\partial T_{II}}{\partial x}\right|_{x=X} - K_{eI}\left.\frac{\partial T_I}{\partial x}\right|_{x=0} = \omega \frac{dX}{dt} \tag{2.7}$$

where ω is defined by

$$\omega = \rho_i \sigma[-\Delta H + C_p(T_0 - T_X)]$$

Since no drying has taken place for $t < 0$,

$$X(0) = 0 \tag{2.8}$$

Note that the energy storage in the dried layer has been neglected in equation 2.7. Also since Region I does not exist at $t = 0$, no initial thermal boundary condition is given.

For Region II

It is assumed that initially Region II is at a temperature T_X, there is no heat transfer to the interface from Region II, and the face at $x = L$ is perfectly insulated. Thus,

$$T(x,t) = T_X \tag{2.9}$$

Solution of Differential System for Case 1

For Region I

Non-dimensionalize equation 2.1 by letting

$$\theta_I = \frac{T_I - T_0}{T_X - T_0} \tag{2.10}$$

With this substitution equation 2.1 becomes

$$\frac{\partial \theta_I}{\partial t} - v \frac{b}{2\sqrt{t}} \frac{\partial \theta_I}{\partial x} = \alpha_{eI} \frac{\partial^2 \theta_I}{\partial x^2} \tag{2.11}$$

Define

$$\eta = \frac{x}{2\sqrt{\alpha_{eI} t}} \tag{2.12}$$

Writing equation 2.11 in terms of η:

$$\frac{d^2\theta_I}{d\eta^2} + \left(2\eta + \frac{vb}{\sqrt{\alpha_{eI}}}\right)\frac{d\theta_I}{d\eta} = 0 \qquad (2.13)$$

Notice that the energy equation has been reduced to an ordinary differential equation in terms of the parameter η. For convenience define

$$U = \frac{1}{2}\left[2\eta + \frac{vb}{\sqrt{\alpha_{eI}}}\right] \qquad (2.14)$$

Substituting equation 2.14 into equation 2.19 and integrating across the dried layer gives:

$$\theta_I = C_3 \frac{2}{\sqrt{\Pi}} \int_0^U e^{-U^2}\, dU + C_4 \qquad (2.15)$$

Recognizing that

$$\frac{2}{\sqrt{\Pi}} \int_0^U e^{-U^2} dU \equiv \text{erf } U = \text{erf } \frac{1}{2}\left[2\eta + \frac{vb}{\sqrt{\alpha_{eI}}}\right] \qquad (2.16)$$

and substituting this definition into equation 2.21 gives

$$\theta_I = C_3 \text{erf}\left[\frac{1}{2}\left(2\eta + \frac{vb}{\sqrt{\alpha_{eI}}}\right)\right] + C_4 \qquad (2.17)$$

Non-dimensionalizing the boundary conditions (equations 2.5 through 2.8) yields:

$$\theta_I(0,t) = 0 \tag{2.18}$$

$$\theta_I(X,t) = 1 \tag{2.19}$$

$$-k_{eI}(T_X - T_0)\left.\frac{\partial\theta_I}{\partial x}\right|_{x=0} = \omega\,\frac{dX}{dt} \tag{2.20}$$

Note that there is no heat flux contribution from Region II so that the term representing this contribution in equation 2.20 has been deleted. Applying equation 2.18 to equation 2.17 results in

$$\theta_I(x,t) = C_3\left(\operatorname{erf}\left[\frac{1}{2}\,\frac{x}{\sqrt{\alpha_{eI}t}} + \frac{vb}{2\sqrt{\alpha_{eI}}}\right] - \operatorname{erf}\left[\frac{vb}{2\sqrt{\alpha_{eI}}}\right]\right) \tag{2.21}$$

Evaluating the derivative of equation 2.21 at x = 0 and substituting into equation 2.20 gives

$$-k_{eI}(T_X - T_0)\,\frac{C_3}{\sqrt{\alpha_{eI}\Pi t}}\exp\left[-\left(\frac{vb}{2\sqrt{\alpha_{eI}}}\right)^2\right] = \omega\,\frac{dX}{dt} \tag{2.22}$$

Notice from equation 2.22 that $\frac{dX}{dt} \sim \frac{1}{\sqrt{t}}$. It is assumed in Appendix A in deriving the energy equation for Region I that $X = b\sqrt{t}$. Differentiating this relationship with respect to t gives $\frac{dX}{dt} = \frac{b}{2\sqrt{t}}$ which indicates that $\frac{dX}{dt} \sim \frac{1}{\sqrt{t}}$. Consequently the assumption made in Appendix A is verified by the form of equation 2.22. Comparing $\frac{dX}{dt} = \frac{b}{2\sqrt{t}}$ to equation 2.22 gives

$$b = -\,\frac{2k_{eI}(T_X - T_0)}{\omega}\,\frac{C_3}{\sqrt{\Pi\,\alpha_{eI}}}\exp\left[-\left(\frac{vb}{2\sqrt{\alpha_{eI}}}\right)^2\right] \tag{2.23}$$

Applying equation 2.19 to 2.23 gives with the additionally established equation $X = b\sqrt{t}$

$$C_3 = \frac{1}{\operatorname{erf} \frac{b}{2\sqrt{\alpha_{eI}}} (1 + \nu) - \operatorname{erf} \frac{b}{2\sqrt{\alpha_{eI}}} \nu} \tag{2.24}$$

Substituting equation 2.24 into equation 2.23 yields

$$b = -2\frac{k_{eI}(T_X - T_0)}{\omega} \left[\frac{1}{\operatorname{erf} \frac{b}{2\sqrt{\alpha_{eI}}} (1 + \nu) - \operatorname{erf} \frac{b}{2\sqrt{\alpha_{eI}}} \nu} \right] \frac{\exp\left[-\left(\frac{\nu b}{2}\right)^2 \frac{1}{\alpha_{eI}} \right]}{\sqrt{\Pi \alpha_{eI}}} \tag{2.25}$$

Equation 2.25 can be solved transcendentally for b. This value of b can be substituted into equation 2.24 to determine C_3. The values of C_3 and b can be substituted into equation 2.21 to yield the temperature distribution. Also the movement of the phase front can be calculated from

$$X = b\sqrt{t}$$

Boundary Conditions for Case 2

For Region 1

The conditions for this region will be the same as those considered for the first case, i.e.

$$T(0,t) = T_0 \tag{2.26}$$

$$T(X,t) = T_X \tag{2.27}$$

$$X\Big|_{t=0} = 0 \tag{2.28}$$

For Region II

A practical case for consideration occurs when the back side of the food sample is heated. The boundary conditions for this case are

$$T_{II}(X,t) = T_X \tag{2.29}$$

$$T_{II}(L,t) = T_L \tag{2.30}$$

Solution of Differential System for Case 2

For Region I

By introducing the non-dimensional parameter given by equation 2.16, equation 2.3 can be transformed to yield

$$\frac{\partial^2\theta_I}{\partial x^2} + \bar{\nu}\frac{dX}{dt}\frac{\partial\theta_I}{\partial x} = 0 \tag{2.31}$$

Similarly transforming equations 2.26 and 2.27 produces the non-dimensional boundary conditions given by equations 2.18 and 2.19 respectively. Integrating equation 2.31 gives the following solution

$$\theta_I = C_5 + C_6 \exp\left(-\bar{\nu}\frac{dX}{dt}x\right) \tag{2.32}$$

Applying the boundary conditions given by equations 2.18 and 2.19 to equation 2.32 results in

$$\theta_I = \frac{1 - \exp\left(-\bar{\nu}\frac{dX}{dt}x\right)}{1 - \exp\left(-\bar{\nu}\frac{dX}{dt}X\right)} \tag{2.33}$$

For Region II

If the parameter given by

$$\theta_{II} = \frac{T_{II} - T_L}{T_X - T_L} \tag{2.34}$$

is substituted into equation 2.4 the following equation results:

$$\frac{d^2\theta_{II}}{dx^2} = 0 \tag{2.35}$$

Integrating gives:

$$\theta_{II} = C_7 x + C_8 \tag{2.36}$$

The transformed boundary conditions are

$$\theta_{II}(X,t) = 1, \qquad \theta_{II}(L,t) = 0 \tag{2.37}$$

Applying these boundary conditions to equation 2.36 gives

$$\theta_{II} = \frac{x - L}{X - L} \tag{2.38}$$

Determination of Interface Position

For case 2 the temperature distributions have been determined in terms of the frozen-dry interface position. In order to determine this position as a function of time, it will be necessary to make an energy balance at the interface, i.e.

$$\left[k_{II}(T_X - T_L)\left.\frac{\partial\theta_{II}}{\partial x}\right|_{x=X^+}\right] + \left[-k_{eI}\left.\frac{\partial\theta_I}{\partial x}\right|_{x=0}(T_X - T_0) - C_p\frac{dX}{dt}\rho_i\sigma(T_0 - T_X)\right]$$

$$= -\sigma\rho_i\frac{dX}{dt}\Delta H \tag{2.39}$$

where the first term is the energy input to interface from region II,

the second term the energy input to interface from region I, and the last term energy required to melt mass flow rate at interface. Differentiating equations 2.33 and 2.38, evaluating these derivatives at x = X and x = 0 respectively, and substituting into equation 2.39 gives on rearrangement

$$\frac{k_{II}(T_X - T_L)}{X - L} - \frac{k_{eI}\,\bar{\nu}\,\frac{dX}{dt}\,(T_X - T_0)}{1 - \exp[-\bar{\nu}\,\frac{dX}{dt}\,X]} = \omega\,\frac{dX}{dt} \tag{2.40}$$

The argument of the exponential term appearing in equation 2.40 is much less in magnitude than one; consequently, the exponential term can be expanded in a Taylor series where only first order terms are retained. Carrying out this procedure, equation 2.40 becomes

$$\frac{X}{B}\,dX - \left[\left(\frac{L}{B} + \frac{\gamma}{B^2}\right)\right]\left[1 - 1\left(\frac{B}{\gamma}\,X + 1\right)\right]\,dX = \omega dt \tag{2.41}$$

where the quantities γ and B are defined below

$$\gamma \equiv L\,k_{eI}(T_X - T_0) \tag{2.42}$$

$$B = k_{II}(T_X - T_L) + k_{eI}(T_0 - T_X) \tag{2.43}$$

Integrating equation 2.41 gives

$$\frac{X^2}{2B} - \left[\frac{L}{B} + \frac{\gamma}{B^2}\right]\left[X + \frac{\gamma}{B}\ln\left(\frac{B}{\gamma}\,X + 1\right)\right] = \omega t + \text{constant} \tag{2.44}$$

Applying equation 2.28 to equation 2.44 yields on rearrangement

$$t = \frac{X^2/2B - \left(\frac{L}{B} + \frac{\gamma}{B^2}\right)\left[X + \frac{\gamma}{B}\ln\left(\frac{B}{\gamma} + 1\right)\right]}{\omega} \tag{2.45}$$

Thus, the complete solution for Case 2 has been obtained. For any time the interface position can be obtained from equation 2.45 by trial and error. With this value of the interface position, the interface velocity can be calculated from equation 2.41. With the known value of interface position and its time derivative, the temperature distribution for Region I can be obtained from equation 2.33 and the distribution for Region II can be obtained from equation 2.38.

Discussion of Assumptions

The effect of the quasi-steady assumption in case 2 was checked by letting the boundary condition at x = L be $T = T_x$. This choice resulted in the same boundary conditions as for case 1. Solutions for actual drying times for both cases with the same boundary conditions were obtained for pressures of 1.0, 2.0, and 3.0 torr. The results for the two cases (one an exact solution and the other solution assuming quasi-steady flow) corresponded within 3 per cent.

In obtaining the solution for case 2, it was assumed that the $\exp(-\bar{v} \frac{dX}{dt} X)$ could be expanded in a Taylor series neglecting the second order terms to give

$$1 - \bar{v} \frac{dX}{dt} X$$

For the usual freeze-drying situation, $\bar{v} \frac{dX}{dt} X$ is approximately equal to 0.1. From knowledge of the Lagrange form of the Taylor series remainder (22),

$$f_{max}^{\bar{k}+1} = \frac{x^{\bar{k}+1}}{(\bar{k} + 1)!}$$

where $f_{max}^{\bar{k}+1}$ is the maximum value of function expanded between 0 and x and $\bar{k}$ is the exponent of the last term kept in the series, it is seen that this assumption results in an error of less than

$$\frac{(0.1)(0.1)^2}{2} \approx 0.0005$$

This is a percentage error of about 0.05 per cent.

CHAPTER III

ANALYTICAL INVESTIGATION OF COUPLED MASS AND HEAT TRANSFER

Determination of Combined Bulk and Diffusional Transport Rate

Introduction

In order to effect a solution an equation must be obtained which will predict the mass transport of a binary gas in the transition regime for the case of simultaneous bulk and diffusional flow under the condition of a non-uniform total pressure gradient. Due to the combination of low pressures and small capillary size the transport occurs in the region between the molecular and viscous condition ($.01 < K_n < 10$). This region will be subsequently referred to as the "transition regime."

To understand the transition regime, first consider the case where the mean free path of the molecules is much less than the characteristic dimensions of the system such as the tube diameter. If a total pressure gradient exists, both components of the binary mixture are transferred by bulk movement of the gas. If, in addition, a concentration gradient exists the movement of each component is superimposed on the bulk movement. At the opposite extreme, when the mean free path is much greater than the characteristic dimension, there is a negligible interaction between the molecules. Consequently the transport is given by Knudsen's (23) equation for molecular streaming under the influence of either a concentration or total pressure gradient. Between these extremes, when the mean free path and the characteristic dimension are

approximately equal, a combination of these transport modes occurs and this phenomena is termed transition flow.

Evans, et al., (24) present equations for combined bulk and diffusional transport in the transition regime under the conditions of a non-uniform total pressure distribution. However, the so called "dusty gas" model was used in which the porous material is idealized as another constituent of immovable large molecules. In addition, the results are valid only for the special case of self diffusion or counter diffusion of gases with equal molecular weight. The current work is concerned with porous materials of a capillaric nature rather than one composed of extremely fine particles for which the dusty gas model is valid. In addition, all flux ratios of the two constituents are considered. A different method (momentum transfer method) is used in the present case to obtain the governing differential equation.

Harper and Chichester (17) state that experimental thermal conductivity data for gases in the transition regime can be used to predict the product of pressure and diffusion coefficient, pD_{12}. They point out that for the continuous flow regime, simple kinetic theory shows that both the thermal conductivity and pD_{12} are independent of pressure. Furthermore, in the transition regime, due to the analogy between heat and mass transfer, both quantities should decrease in a similar manner with decreasing pressure. However, the continuous flow regime, Present (25) notes that the simple kinetic theory expression giving thermal conductivity to be independent of pressure gives excellent agreement with experimental data. The corresponding development for pD_{12} shows that it should be independent of pressure but heavily dependent on the concentration of the gaseous

components; this expression for pD_{12} cannot be experimentally substantiated. The dichotomy between the simple kinetic theory expression and experimental data results from the basic difference between the nature of the transport of mass and energy. For energy transfer across a given plane, the specific identity of the component molecules (either component 1 or component 2) is not important, whereas for mutual diffusion, the identity of the molecules is quite important. The mass transfer depends in part on whether the molecules collide with like or unlike molecules before crossing the plane. The collision of like molecules prior to crossing the plane does not affect the diffusive transport process, but it is greatly affected if unlike molecules collide. Thus since the two mechanisms of transfer are not exactly analogous in the continuous flow regime, it appears unlikely that they would be analogous in the transition regime. It is desirable, therefore, to analytically and experimentally examine the assumption made by Harper and Chichester for combined bulk and diffusion flow of a binary gas mixture. Small total pressure and concentration gradients are assumed to exist simultaneously.

Consequently, it is desired to obtain analytical results for the rate of mass transfer under the above conditions for flow through a capillary tube. These results will be modified for the case of transport of an air water-vapor mixture through porous freeze dried beef for use in predicting drying rates.

Analytical Investigation

Johnson (26) suggests that the steady diffusion equation for continuous transport can be interpreted as an equation of motion of one of the constituent gases. The equation in the form of an equation of motion

valid for the one dimensional transport of a binary gas at uniform total pressure is;

$$F_2\,dx - d\bar{p}_2 - \frac{KT}{n_M D_{12}}\, n_1 n_2 (u_2 - u_1)dx = 0 \qquad (3.1)$$

The first term in equation 3.1 is the total external force per unit area on component 2, the second term is the force per unit area on component 2 due to a partial pressure gradient and the third term is the momentum transfer to component 2 due to collisions with component 1.

If a small total pressure gradient exists, the Maxwell-Boltzmann distribution function evaluated at the average pressure is very nearly the same as for the uniform pressure case. Therefore, the last term in equation 3.1 still adequately describes the momentum exchange between the two constituents. However, the total pressure gradient causes an effective external force on component 2 which is equal to the product of the total pressure gradient and the average area occupied by this component. From Dalton's law, it can be easily shown that the cross-sectional area of component 2 is

$$A_2 = \pi R^2 \frac{\bar{p}_2}{p} \qquad (3.2)$$

Since the net force on component 2 due to the total pressure gradient is $A_2 dp$, equation 3.1 can be written

$$\bar{p}_2 dp/p - d\bar{p}_2 = \frac{KT}{n_M D_{12}}\, n_1 n_2 (u_2 - u_1)dx \qquad (3.3)$$

Equation 3.3 is valid for continuous flow when only intermolecular interactions are important. For transitional flow, one must consider molecular encounters with the wall; therefore, equation 3.3 must be altered to include the resulting momentum exchange with the wall. From kinetic theory, the number of molecules striking the inside of the capillary surface per unit time is $\pi r_c n_2 \bar{V}_2 dx/2$. If diffuse reflections occur, the average velocity change resulting from a molecular collision with the wall is u_2. In general, the average velocity change is $u_2 S$, where S is the reflection coefficient, defined as the number of molecules striking a unit area with completely diffuse momentum exchange divided by total number of molecules striking the unit area. Therefore, the momentum exchange with the wall for each molecule is $n_2 u_2 S$. Taking this into consideration, equation 3.3 becomes

$$(\bar{p}_2/p)dp - d\bar{p}_2 = \frac{KT}{n_M D_{12}} n_1 n_2 (u_2 - u_1)dx + S m_2 u_2 n_2 \bar{V}_2 dx/2r_c \qquad (3.4)$$

This equation is the final form of the differential equation of motion for one component of a binary gas mixture. It is valid for the case of combined bulk and diffusional flow in the transition regime under the condition of a non-uniform total pressure gradient.

An expression for the average molecular velocity can be determined from kinetic theory if a Maxwellian distribution is assumed. This expression is

$$\bar{V}_2 = (8KT/\pi m_2)^{1/2} \qquad (3.5)$$

Since

$$\bar{p}_2 \frac{dp}{p} - d\bar{p}_2 = -pd\left(\frac{\bar{p}_2}{p}\right) = -pdy_2 \tag{3.6}$$

Equation 3.4 can be combined with equations 3.5 and 3.6 to give

$$\frac{-pdy_2}{RT} = N_2 \left[\frac{8S}{3\pi D_{K2}} + (n_1 - n_2 \frac{N_2}{N_1})/n_M D_{12}\right] dx \tag{3.7}$$

From Dalton's law of partial pressures,

$$y_1 + y_2 = 1.0 \tag{3.8}$$

and making use of the definition of a, y_1 and y_2, and substituting equation 3.8 into equation 3.7 gives

$$N_2 dx = -\frac{pD_{12}dy_2}{\tilde{R}T} \Big/ \left[1 - ay_2 + \frac{8SD_{12}}{3\pi D_{K2}}\right] \tag{3.9}$$

For the small pressure gradients considered, it is assumed that p can be expanded in a Taylor series neglecting the 2d order terms to give

$$p = p_0 + \frac{dp}{dx} x \tag{3.10}$$

Approximating $\frac{dp}{dx}$ by $\frac{\Delta p}{L}$ gives

$$p = p_0 + \frac{\Delta p}{L} x \tag{3.11}$$

From kinetic theory

$$\frac{pD_{12}}{\tilde{R}T} = C_q \tag{3.12}$$

where C_q is a constant. From the definition of z,

$$dx = Ldz \tag{3.13}$$

Substituting equations 3.10-3.13, into equation 3.9 gives on rearrangement,

$$\frac{dy_2}{dz} - \frac{N_2 La}{C_q} y_2 = - \frac{N_2 L}{C_q} \left[1 + \frac{8S}{3\pi D_{K2}} \frac{C_q \tilde{R} T}{p_0 + \Delta p z} \right] \tag{3.14}$$

Substituting the definitions of b_4 and b_3 into equation 3.14, integrating and applying the boundary conditions $y_2 = y_{20}$ at $z = 0$ and $y_2 = y_{2L}$ at $z = 1$ gives

$$y_{2L} = \frac{1}{a} \tag{3.15}$$

$$+ \frac{b_3}{\Delta p} \frac{\log(p_0+\Delta p)+[b_4(1+\frac{p_0}{\Delta p})]+ \frac{1}{(2)2!}[b_4(1+\frac{p_0}{\Delta p})]^2+ \frac{1}{(3)3!}[b_4(1+\frac{p_0}{\Delta p})]^3+ \ldots}{\exp[b_4(1 + p_0/\Delta p)]}$$

$$+ \frac{y_{20} - \frac{1}{a} - \frac{b_2}{\Delta p} \exp(-\frac{p_0}{\Delta p} b_4) \log p_0 + \frac{1}{(2)2!}(\frac{b_4}{\Delta p} p_0)^2 + \frac{1}{(3)3!}(\frac{b_4}{\Delta p} p_0)^3 + \ldots}{\exp(b_4)}$$

The series contained in the braces converges for all values of $b_4 \frac{p_0}{\Delta p}$ and $b_4(p_0 + \Delta p)/\Delta p$. It is convenient to define an average diffusion coefficient D_t for the transition regime by means of the following equation:

$$N_2 = \frac{pD_t}{\tilde{R} TLa} \ln \frac{1 - y_{2L}}{1 - y_{20}} \tag{3.16}$$

Equations 3.15 and 3.16 can be solved by the following trial and error procedure. First assume a value of D_t and then calculate the

corresponding value of N_2 from equation 3.16. Next use this value of N_2 to calculate y_{2L} from equation 3.15 and then compare the magnitude of the calculated value of y_{2L} with the known value from the boundary condition of the tube exit. This procedure can be repeated until the correct value of D_t is obtained.

Application to Flow in Freeze-Dried Beef

Freeze-dried beef contains numerous small voids which form complex flow paths for vapor transport. These flow paths are non-uniform in cross section and are not straight. The method used for analyzing this case is to assume the voids form circular and straight capillaries. However, for actual substances, the analytical equations resulting from these assumptions should be altered to include the effects of devious flow paths and blockages caused by the structure of the porous sample. Parameters which account for these irregularities are called "effective parameters."

The analytical results presented in the previous section can be used for actual porous meat in obtaining the magnitude of the effective diffusion coefficient if the values of D_{12} and D_{K2} used in the definitions of b_3 and b_4 are the effective values for the porous sample. For the application to freeze-drying component 1 will be considered air and component 2 water vapor. Effective values are defined so that the vapor flux can be written in terms of the total sample area and its actual thickness. Due to the complexities of the structure of porous materials, the effective values of D_{12} and D_{K2} are not predicted analytically; but, instead, are measured experimentally. In order to reduce the amount of experimental data required, Scott and Dullien (14) suggest that

$$\frac{(D_{aw})_e}{(D_{kw})_e} = \frac{D_{aw}}{D_{kw}} \tag{3.17}$$

Thus, by obtaining the value of $(D_{aw})_e$ by a single experiment, the value of $(D_{kw})_e$ can be calculated by substituting the experimental value of $(D_{aw})_e$ and the known values of D_{aw} and D_{kw} into equation 3.17. To calculate a theoretical value for $(D_t)_e$ for the porous sample, the values of $(D_{aw})_e$ and $(D_{kw})_e$ are used to obtain b_4 and b_3 from their definitions, and then equations 3.15 and 3.16 are solved by the iteration procedure previously described.

Equation 3.16 is the equation of motion for the water-vapor species. Rewritten in terms of the nomenclature used for the freeze drying process, equation 3.16 becomes

$$N_w = \frac{p(D_t)_e}{\tilde{R}\,TXa} \ln \frac{1 - y_{20}}{1 - y_{2X}} \tag{3.18}$$

The value of "a" is obtained by writing the continuity equation for the air species and making the quasi-steady assumption. When integrated this equation is

$$N_a = C_{10} \tag{3.19}$$

Where C_{10} is a constant. But at the interface ($x = X$) $N_a = 0$. Therefore from equation 3.19, $C_{10} = 0$ and $N_a = 0$ for all positions. Substituting the value of N_a into the definition of "a" gives

$$a = 1$$

Consequently, the equation of motion for the water vapor species becomes

$$N_w = \frac{p(D_t)_e}{\tilde{R}\ TX} \ln \frac{1 - y_{20}}{1 - y_{2X}} \tag{3.20}$$

Equations of Continuity, Motion, and Energy for the Mixture

These equations have already been obtained in appendicies A and B. However each equation must be changed from a mass basis to a molar basis for use with equation 3.20. The equation of continuity given in Appendix B becomes on changing to a molar basis making the quasi-steady assumption, integrating, and noting $N_a = 0$

$$N_w = C_{11} \tag{3.21}$$

where C_{11} is a constant.

In considering the momentum equation for the gaseous mixture the results of the derivation in Appendix B are seen to be applicable since the Navier Stokes equations for a gaseous mixture are the same as the equations for a pure gas if external forces on the individual species are neglected. Thus, since for this case no external forces act, the equation of motion for the mixture is equation B.38. Rewriting this equation in terms of the nomenclature used for the freeze-drying process and on a molar basis gives

$$\frac{N_w X}{\Delta p} = -\varepsilon\ (p_m) M_w \frac{\rho}{\nu} \tag{3.22}$$

where $\varepsilon(p_m)$ has been determined by experiment. Values of $\varepsilon(p_m)$ as a function of pressure are given in Appendix C. For convenience define

$$\tilde{\varepsilon} = -\varepsilon(p_m)M_w \frac{\rho}{\nu} \tag{3.23}$$

Equation 3.22 becomes

$$N_w = \tilde{\varepsilon} \frac{\Delta p}{X} \tag{3.24}$$

The energy equation for Region I is derived in Appendix B. The quasi-steady assumption is envoked which will give in non-dimensional form the energy equation used for case 2 of Chapter II, i.e.

$$\frac{d^2\theta_I}{dx^2} - W_w \frac{C_p}{k_{eI}} \frac{d\theta_I}{dx} = 0 \tag{3.25}$$

W_w can be written on a molar basis if C_p is written on the same basis. Thus

$$\frac{d^2\theta_I}{dx^2} - N_w \frac{\tilde{C}_p}{k_{eI}} \frac{d\theta_I}{dx} = 0 \tag{3.26}$$

From equation B.26 it is seen that the coefficient of $d\theta_I/dx$ is independent of x. The non-dimensional energy equation for Region II is the same as used for case 2, Chapter II.

$$\frac{d^2\theta_{II}}{dx^2} = 0 \tag{3.27}$$

Boundary Conditions

The thermal boundary conditions at the heated and back side are respectively

$$\theta_I(0) = 0 \tag{3.28}$$

$$\theta_{II}(L) = 0 \tag{3.29}$$

An energy balance and temperature-partial pressure relationship at the interface (x = X) gives the following two equations respectively

$$\left[k_{II}(T_X - T_L)\left.\frac{d\theta_{II}}{dx}\right|_{x=X}\right] + \left[-(T_X - T_0)k_{eI}\left.\frac{d\theta_{II}}{dx}\right|_{x=0}\right] \tag{3.30}$$

$$- \tilde{C}_p N_2(T_0 - T_X) = -N_2\Delta\tilde{H}$$

$$\bar{p}_w(X) \equiv \bar{p}_{wX} = f(T_X) \tag{3.31}$$

where $f(T_X)$ is a function of the interface temperature. This function has been experimentally determined and is presented as equation 5.7 in Chapter V. Putting the experimentally determined expression for $f(T_X)$ in equation 3.31 gives

$$\bar{p}_{wX} = \exp\,(27.70 - 12900.0/T_X) \tag{3.32}$$

The known values of the chamber pressure p_0 and the water-vapor partial pressure $\bar{p}_{w0}$ give the final boundary conditions

$$p\big|_{x=0} = p_0 \tag{3.33}$$

$$\bar{p}_w\big|_{x=0} = \bar{p}_{w0} \tag{3.34}$$

Solution of Differential Set

Equations 3.20, 3.24, 3.26 and 3.27 must be solved with the

boundary conditions equations (3.28-3.34). The temperature distributions obtained by integrating equations 3.26 and 3.27 are

$$\theta_I = \frac{1 - \exp(-N_w \tilde{C}_p x/k_{eI})}{1 - \exp(-N_w \tilde{C}_p X/k_{eI})} \tag{3.35}$$

$$\theta_{II} = \frac{x - L}{X - L} \tag{3.36}$$

Differentiating equations 3.35 and 3.36 and substituting into equation 3.30 gives

$$\frac{k_{II}(T_X - T_L)}{X - L} - \frac{k_{eI}(T_X - T_O)N_w \tilde{C}_p/k_{eI}}{1 - \exp(-N_w \tilde{C}_p X/k_{eI})} = N_w[-\Delta \tilde{H} + \tilde{C}_p(T_O - T_X)] \tag{3.37}$$

Expanding the exponential terms in equation 3.37 in a Taylor series gives on rearrangement

$$N_w X = \frac{\frac{X}{X - L} k_{II}(T_X - T_L) - k_{eI}(T_X - T_O)}{-\Delta \tilde{H} + \tilde{C}_p(T_O - T_X)} \tag{3.38}$$

From equations 3.32 through 3.34, and the definition of mole fraction,

$$y_{wO} = \bar{p}_{wO}/p_O \tag{3.39}$$

$$y_{wL} = \bar{p}_{wX}/p_X = \frac{\exp(27.70 - 12900/T_X)}{p_O + N_w X/\tilde{\varepsilon}} \tag{3.40}$$

Substituting equations 3.38, 3.39 and 3.40 into equation 3.20 gives

$$\frac{k_{\Pi}\frac{X}{X-L}(T_X - T_L) - k_{eI}(T_X - T_O)}{-\Delta\tilde{H} + \tilde{C}_p(T_O - T_X)} \tag{3.41}$$

$$= \frac{pD_t}{\tilde{R}T}\ln\frac{1 - \frac{\bar{p}_{wO}}{p_O}}{1 - \left[\frac{\exp(27.70 - 12900/T_X)}{\frac{\frac{k_{\Pi}(X)}{X-L}(T_X-T_L) - k_{eI}(T_X-T_O)}{[-\Delta\tilde{H} + \tilde{C}_p(T_O - T_X)]\tilde{\varepsilon}} + p_O}\right]}$$

For any interface position this equation can be solved by trial and error for the value of T_x. The molar flow rate is given by

$$N_w = \lim_{\Delta t \to 0} \frac{X\Big|_{t+\Delta t} - X\Big|_t}{\Delta t}\tilde{\rho}_i\sigma \tag{3.42}$$

Consequently for a small interface movement ΔX in a time Δt

$$N_w \approx \frac{\Delta X}{\Delta t}\tilde{\rho}_i\sigma \tag{3.43}$$

A numerical technique can be used to obtain the drying time by the following procedure:

(1) Calculate T_x for small increments of x from equation 3.41 by trial and error.

(2) Use the corresponding values of T_x and X to calculate N_w from equation 3.38 for each of the interface positions.

(3) Rearrange equation 3.43 in the form

$$t \approx \frac{\Delta X\ \rho_i\sigma}{N_w}$$

to calculate the time required for the incremental change in interface position.

(4) Add up all the increments of time to obtain the total drying time.

It should be noted that since the properties change slowly with time relatively large incremental changes in interface position can be used with good approximation.

Special Case

The solution to the differential set is greatly simplified when $T_L = T_X$. For this case T_X is a constant and can be obtained by setting $T_L = T_X$ in equation 3.41 which yields

$$\frac{k_{eI}(T_0-T_X)}{-\Delta\tilde{H}+\tilde{C}_p(T_0-T_X)} = \frac{pD_e}{\tilde{R}\,T} \ln \frac{1-\dfrac{\bar{p}_{w0}}{p_0}}{1-\left[\dfrac{\exp(27.70-12900/T_X)}{p_0+\dfrac{k_{eI}(T_0-T_X)}{\tilde{\varepsilon}[-\Delta\tilde{H}+\tilde{C}_p(T_0-T_X)]}}\right]} \tag{3.44}$$

The value of $N_w X$ can be calculated from equation 3.38 by setting $T_L = T_X$ and substituting in the value of T_X. Note that the magnitude of $N_w X$ is a constant which will be denoted by C_{15}. The relationship between the flow rate and interface velocity is

$$N_w = \tilde{\rho}_i \sigma \frac{dX}{dt} \tag{3.45}$$

Substituting $N_w = \dfrac{C_{15}}{X}$ into equation 3.45, integrating and noting that at $t = 0$, $X = 0$ gives

$$t = \frac{\tilde{\rho}_i \sigma X^2}{2C_{12}} \tag{3.46}$$

The drying time can be obtained by letting X = L in equation 3.46.

CHAPTER IV

EXPERIMENTAL INVESTIGATIONS

Vapor Pressure Measurement

Instrumentation and Equipment

The equipment used for this measurement is shown in Figure 2. The equipment was designed such that measurements can be made on a frozen beef sample or on the frozen liquid squeezed from the beef sample. The vacuum flask had a volume of 2000 millimeters and was submerged as shown in a bath of acetone. In order to obtain true equilibrium vapor pressures, it was necessary to maintain this bath at the temperature at which the vapor pressure is desired. To produce these temperatures, a refrigeration unit was construced using a Copeland* model KG 0050 IAA compressor unit. A Welch** model number 1402 mechanical vacuum pump was used to evacuate the vacuum flask.

The pressure was measured by means of a Wallace and Tiernan*** type 160 absolute pressure gage. The calibration curve furnished by the factory was used to correct the pressure readings.

The temperature in the sample was recorded at two points within the sample by use of copper-constantan 28 gage thermocouple wire. The thermocouple output was measured by use of a portable potentiometer used in conjunction with a thermocouple multiple switch. The

---

* Copeland, Sidney Ohio.

** W. M. Welch Scientific Co., 7300 N. Linder Avenue, Skokie, Illinois.

*** Wallace and Tiernan, Incorporated, 25 Main Street, Belleville 9, New Jersey.

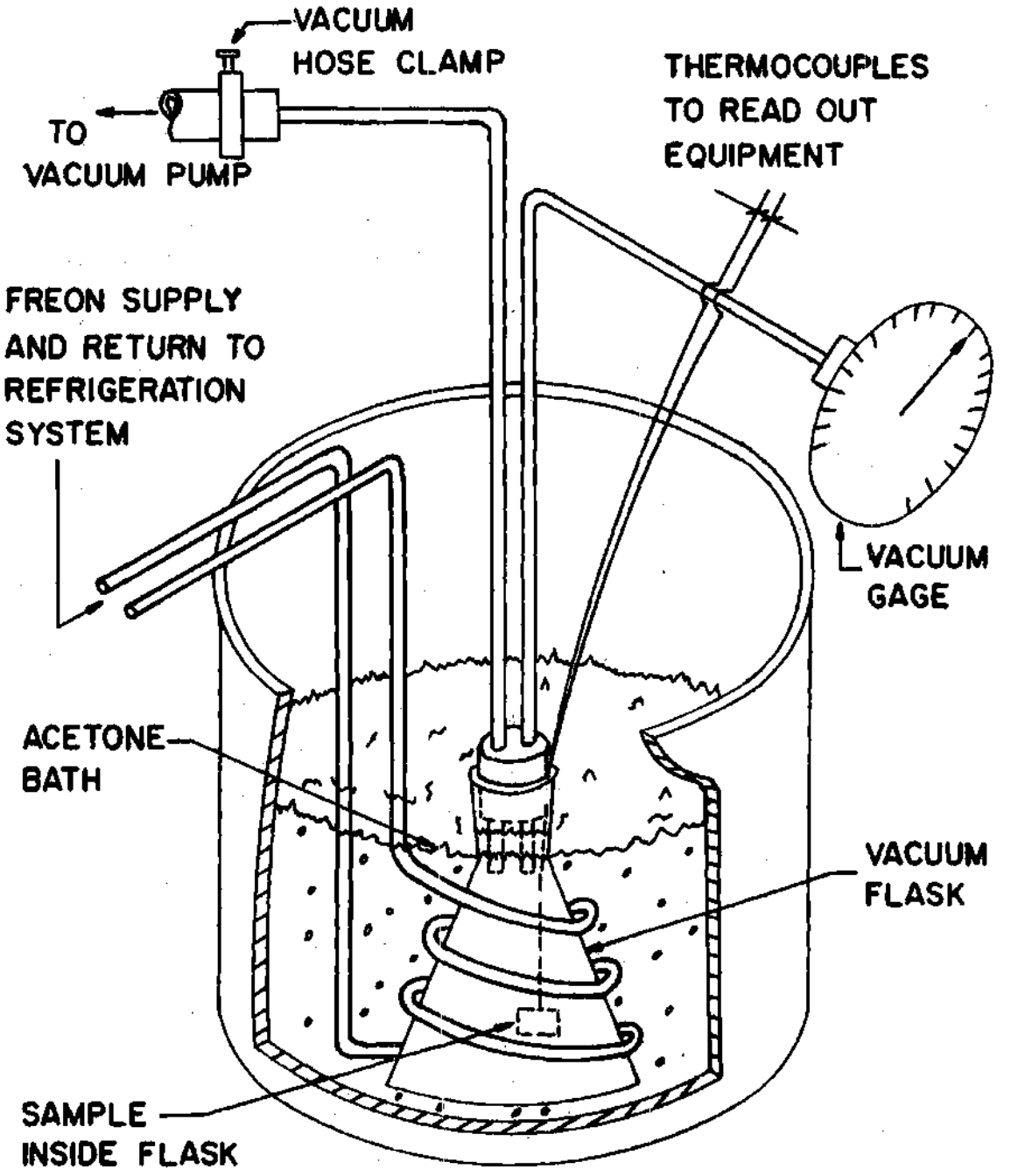

Figure 2. Experimental Apparatus for Vapor Pressure Determination.

temperature sensing apparatus was calibrated against a secondary standard mercury-in-glass thermometer.

Procedure

The following steps were taken to obtain vapor pressure data:

1. The vacuum system (see Figure 2) was assembled and pumped for approximately one day in order to remove contaminants without the sample being included and without refrigerating the acetone bath.

2. The refrigeration system was then started.

3. For tests on solid meat samples two thermocouples were located in the meat and the meat was then frozen. The sample size used was approximately 1/2 by 1.0 by 3/4 inches. For tests of the liquid squeezed from the meat sample, the liquid was placed in a small glass cylindrical capsule (approximately 1/2 inch diameter by 3/4 inches deep) with one end open. Thermocouples were secured in the proper position and the liquid frozen.

4. The sample was then placed in the vacuum flask. Since the thermocouple wires were extremely small in diameter, it was possible to feed the wires out between the rubber stopper and the vacuum flask wall without introducing leaks. The stopper was then replaced in the flask.

5. The mechanical pump was started and the system pumped to a low pressure (approximately 0.3 torr). Note that this allowed a slight amount of residual air to remain in the flask.

6. The acetone bath was allowed to reach the temperature at which the vapor pressure measurement was desired and then to stabilize.

7. The hose clamp located between the pump and flask was then closed.

8. The sample was allowed to come into temperature equilibrium with the external bath. This was determined by comparing the two thermocouple readings of the sample with a mercury-in glass thermometer reading of the bath temperature.

9. The pressure in the flask was then read.

10. In order to determine the residual air pressure, dry ice was introduced into the acetone bath. The low temperatures produced by the dry ice froze the water-vapor onto the inside walls of the flask. The temperature and pressure inside the flask were read. By using Dalton's law of partial pressures and the ideal gas law as described by reference (27), the new pressure obtained can be converted into the partial pressure of the residual air. Then the actual vapor pressure is the total pressure initially read minus the computed air residual pressure.

It should be noted that after it was established that the leak rate for the apparatus was very small, step 10 was carried out to determine the initial residual air pressure. Then several data points were taken as described in the first nine steps for different temperatures by slowly allowing the acetone bath temperature to change (thus, changing the sample temperature). The residual amount of air pressure was again determined by step 10 and the leak rate calculated from the known initial and final air pressure. The data taken between the initial and final determination of the residual air pressure were corrected by means of the known leak rate.

Discussion of Experimental Accuracy

The overall accuracy of the experimental set-up was investigated by measuring the vapor pressure of pure ice. Measurements were made

over the same range that was examined for the food product. The results of this check corresponded to published vapor pressure data for pure ice within one per cent.

Permeability Coefficient Measurement

Instrumentation and Equipment

From the derivation in Appendix B, it is seen that the permeability correlation (equation B.38) involves the measurement of the physical dimensions (area and thickness) of the freeze-dried porous beef, the mass rate of flow through the porous media, the average total pressure, and the resulting total pressure drop. Two methods were used to obtain this necessary data.

First Method. The first method involved the use of the equipment shown in Figure 3. The test chamber (see Figure 3) was constructed from schedule 40 stainless steel pipe and had an internal diameter of 6 inches and height of 15 inches. Rubber o-rings were used to provide the vacuum seal. A by-pass valve and a flow regulation valve to the pump were provided and were obtained commercially from the NRC Equipment Corporation. A hollow circular ring was provided for holding the meat sample. This ring could then be sealed across the cross section of the test chamber as shown in Figure 3.

The absolute pressure in the lower half of the chamber was measured by means of a Wallace and Tiernan Type 160 vacuum pressure gage. The differential pressure was obtained by inclining a u-tube manometer

---

* NRC Equipment Corporation, 160 Charlemont Street, Newton Highland 61, Massachusetts.

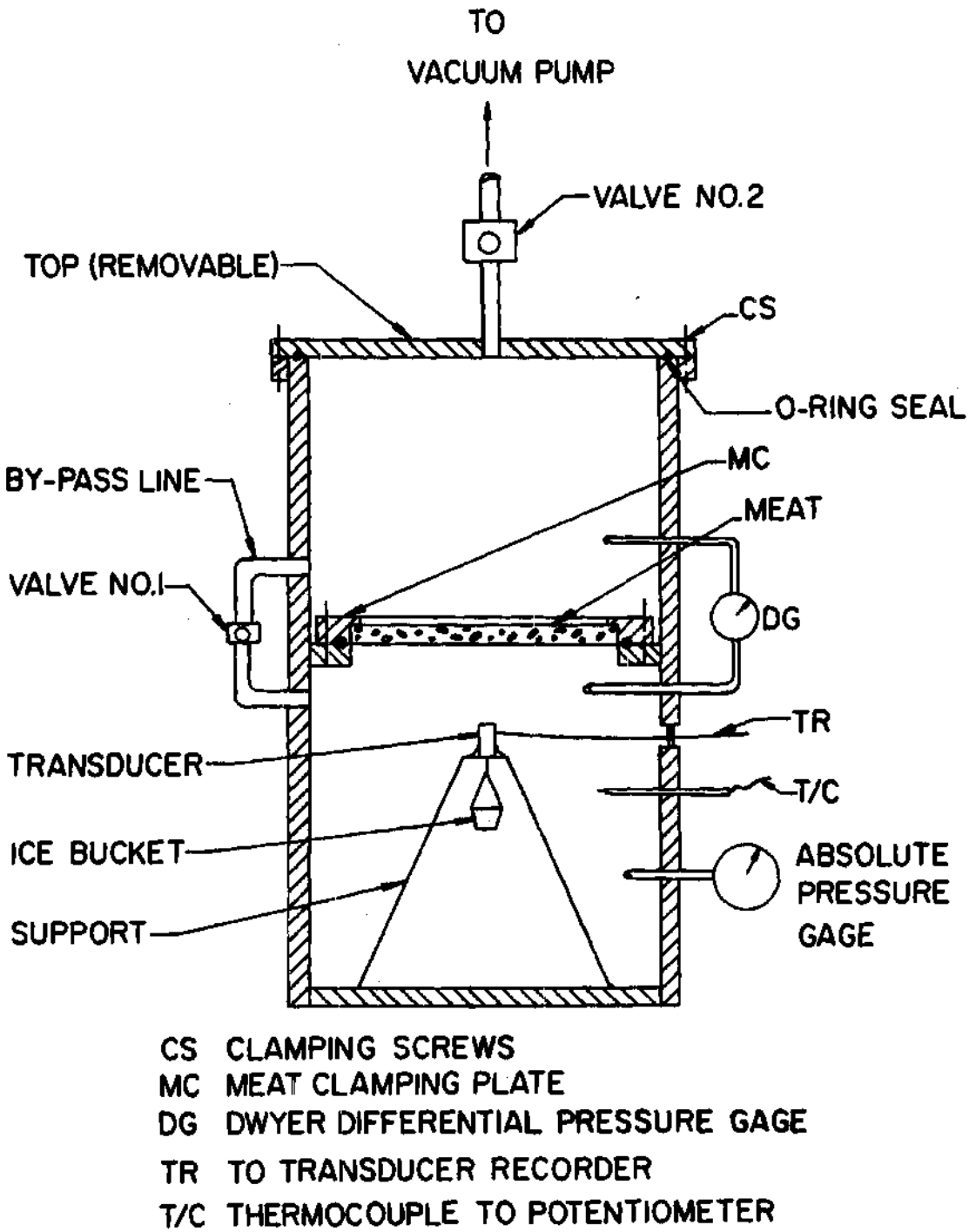

Figure 3. Apparatus for Determining Permeability -First Method.

and using Dow Corning* 200 fluid. This fluid has an extremely low vapor pressure (about 10^{-6} torr) and a specific gravity of nearly 1.0. Thus, with this arrangement extreme sensitivity was obtained.

The sublimating ice was contained in a cup suspended for a Sanborn** model FTA-10-1 transducer. The ice was a sufficient distance from the bottom surface of the sample to insure that the flow through the sample was approximately isothermal. The electrical output of the transducer was fed into a Sanborn model 296 amplifier and the amplifier signal was monitored on a Hewlett Packard*** model number 405 CR digital volt meter. The voltmeter output was calibrated in terms of the weight applied to the transducer. Thus, from monitoring the weight loss versus time the flow rate could be determined.

A Welch model number 1402 mechanical vacuum pump was used for evacuating the chamber and pumping the sublimating ice through the sample.

Second Method. The apparatus used for the second method is shown in Figure 4. The main vacuum chamber housing the test section was large (approximately a cube with 2.5 ft. edges). The vapor was pumped by a condenser which was connected to the chamber by a 6 inch diameter pipe. The condenser opened to the vacuum pump (Welch model number 1410). Acetone and dry ice were used as the condenser refrigerant. Flow regulation valves manufactured by the NRC Equipment Corporation were provided between the main chamber and condenser and the condenser and vacuum pump.

---

*Dow Corning Corporation, Midland, Michigan.

**Sandborn Company, Waltham 54, Massachusetts.

***Hewlett-Packard Company, 1501 Page Mill Road, Palo Alto, California.

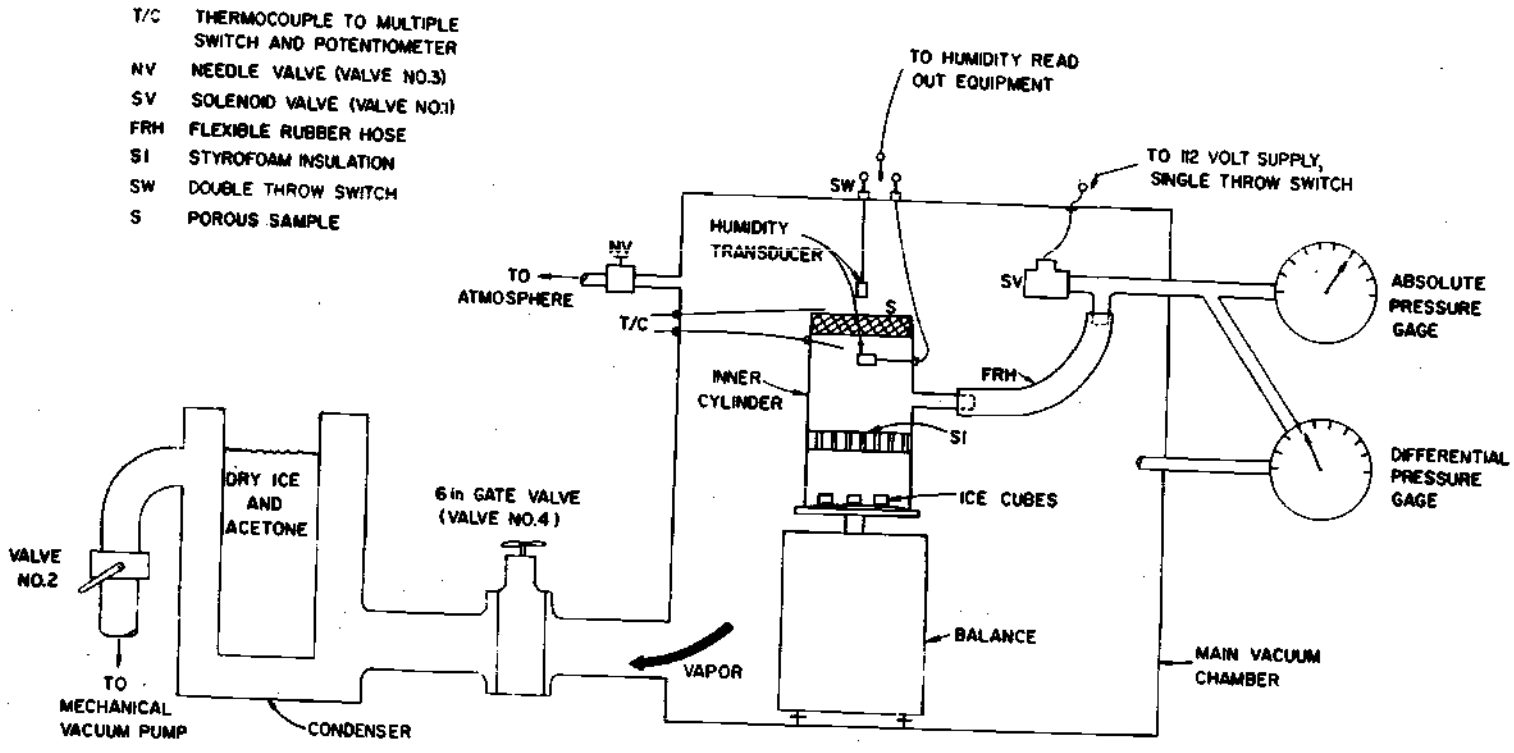

Figure 4. Apparatus for Determining Permeability — Second Method.

In addition, a needle valve opening to the atmosphere was provided for regulation of chamber conditions. The test section was constructed from a light gage steel cylinder (approximately 4 in diameter by 6 in high). During pump down it was required that the inside of the test section be opened to the main vacuum chamber in order to evacuate the test section. A by-pass line opening to the main vacuum chamber, as shown in Figure 4, was provided from the inside of the test section. This line could be opened or closed with a solenoid valve (Valve No. 1). This allowed the test section to be pumped down simultaneously with the main chamber.

The absolute pressure of the main vacuum chamber was determined by means of a calibrated Wallace and Tiernan Type 160 vacuum absolute pressure gage. The differential pressure across the sample was measured with a Dwyer* "magnehelic" differential pressure gage. The temperature above and below the sample was monitored by copper constantan thermocouples.

The ice for sublimation was placed in the bottom of the test section. A one inch thick piece of styrofoam with small holes punched through it was provided for thermal insulation between the ice and bottom surface of the sample to insure essentially isothermal flow. The weight of the test section, meat sample, and ice was obtained by use of a Mettler type KST CD balance.

Procedure

The procedure for each method used to obtain the necessary data for calculating the permeability is given below.

*F. W. Dwyer Manufacturing Company, P. O. Box 373, Michigan City, Indiana.

First Method.

1. The sample was sealed in the circular holder and the holder was secured by socket screws across the test section. The top of the test chamber was also assembled by means of set screws.

2. Valve 1 (see Figure 3) was completely opened and the vacuum pump started. Valve 2 was opened slightly for evacuation of the chamber. Care was taken to keep the pumping rate low enough that only a small differential pressure existed across the sample.

3. The system was pumped for some time to ensure that a negligible amount of air remained in the tank after which valve 1 was closed.

4. The water-vapor was pumped through the sample until the pressures above and below the sample became constant. When these conditions were achieved the differential pressure, absolute pressure, weight and time were recorded by means of the equipment described above.

5. The test was conducted for a time of 10 minutes after which the differential pressure, absolute pressure, and weight were again recorded.

The data taken in steps 4 and 5 along with the physical dimensions of the meat sample provided the information described above which was required to calculate the permeability.

Second Method.

1. The condenser was charged with dry ice and acetone.

2. The freeze-dried porous sample was sealed across the top of the test section.

3. The solenoid valve (valve number 1 in Figure 4), and valves 2 and 4 were opened and the chamber door closed. The chamber was then pumped to a low pressure and held at this pressure in order to assure

that negligible air remained in the system. Valve 1 was then closed.

4. Valve 4 was adjusted to give the desired back pressure (main chamber pressure).

5. After allowing time for the pressures above and below the sample to stabilize, readings of absolute chamber pressure, temperature, differential pressure across the sample, and weight of test section, meat sample and ice were recorded at a known time.

6. After an elapsed time of 1 hour these readings were repeated.

Since the test section and meat sample did not change weight, the measured loss in weight corresponded directly to the mass rate of water-vapor flowing through the meat. With this flow rate, the pressure drop across the sample, the chamber absolute pressure, temperature, and physical dimensions of the sample, the necessary information for calculating the permeability was provided.

Comparison of Two Methods

Some explanation for using two measuring techniques seems in order. The transducer used in the first method was very sensitive and accurate; consequently, only short runs were required to obtain accurately the mass flow rate. However, it was questionable whether all of the sublimating water leaving the cup passed through the sample since part of the water-vapor could have condensed in the meat sample. Therefore, the second method was devised to circumvent this problem. Note that with this method only the loss of water-vapor that passes through the meat is measured. However, a disadvantage of this method is that a much longer period of time was required for a run since the weighing means were much less sensitive.

Another problem encountered with the first method provided additional impetus for devising a new method. It was found to be impossible to obtain the desired range of absolute pressure and differential pressure with the equipment used in the first method. The second method proved to provide the desired range of absolute pressure and differential pressure.

In summary, the first method provided fast results while the second method provided slower results but with the advantage that wider ranges could be investigated with the assurance that the flow rate obtained was accurate. The majority of the data in this investigation was obtained using the second method, although for average pressure of about 1 torr several points were taken using the first method. The method for obtaining the permeability data appearing in Appendix C is clearly shown.

Discussion of Experimental Accuracy

Results from the two methods were compared and found to coincide within a close percentage. In addition the results of this investigation were compared with the results of references (16) and (17) and were found to lie intermediate between the values found in these two references.

Mutual Diffusion Coefficient Measurement

Instrumentation and Equipment

The equipment used for this part of the investigation was a modification of the equipment applied in the second method for determining the permeability coefficient (equipment shown in Figure 4).

The modification involved the addition of two humidity transducers -- one Hygrodynamics* model 4-4812 located above and one Hygrodynamics model 4-4814 located below the porous dried sample as shown in Figure 4. The electrical leads of the transducers were fed through the main vacuum chamber and connected to a double throw electrical switch which in turn was connected to a Hygrodynamics model 15-3000 humidity read-out instrument. By selecting the appropriate position of the switch the humidity above or below the sample could be monitored on the read-out equipment.

The derivation of the diffusion equation given in Chapter III indicates the need for the addition of the humidity transducers, since in addition to the data required in the permeability tests, the water-vapor concentration above and below the sample is required for calculating the diffusion coefficient.

Procedure

1. The condenser was charged with dry ice and acetone.

2. The freeze-dried porous sample was sealed across the top of the test section.

3. The solenoid valve (valve number 1 in Figure 4), and valves 2 and 4 were opened and the chamber door closed. The chamber was then pumped to a pressure of approximately 0.7 torr.

4. The desired amount of air was admitted through valve 3.

5. The solenoid valve was closed, valve 4 was adjusted to give the desired chamber pressure, and time was allowed for equilbrium to be obtained.

*Hygrodynamics, Inc., 949 Selim Rd., Silver Spring, Maryland.

6. Readings of chamber pressure, differential pressure across the sample, water-vapor concentration above and below the sample, and the weight of test section, meat sample and ice were recorded at a known time.

7. After an elapsed time of 1 hour these readings were repeated.

From these measurements the vapor flow rate could be calculated as for the permeability coefficients. With this flow rate, the pressure drop across the sample, the chamber absolute pressure, the concentrations above and below the sample, and the physical dimensions of the sample, the average diffusion coefficient could be calculated from equation 3.16.

Discussion of Experimental Accuracy

Since the diffusion measurement required the determination of several quantities, the propogated expected error could be expected to be rather large. However, since each of the measuring devices were calibrated, the individual error associated with each measurement was generally under 2 per cent giving a progated expected error of approximately 10 per cent. The variations in the properties of the samples used have been found to be of the same order. Consequently, the equipment was sufficiently accurate from a practical standpoint.

Determination of Thermal Transpiration Effect

Instrumentation and Equipment

Kinetic theory shows that a temperature gradient causes an additional mass flux as compared to the case of isothermal flow. To experimentally investigate this effect, the data for the permeability tests were compared to results for the same type test with the exception that

a thermal gradient was imposed. Consequently, the equipment used for this study was the same as for the permeability test (second method, see page 41) with the exception that a radiant heater was installed above the sample and the styrofoam insulation between the ice and bottom of sample was removed.

Procedure

The procedure used was the same for the permeability measurements except that the heater mentioned above was turned on before the beginning of the experiment.

Discussion of Experimental Accuracy

Since the additional temperature measurements required in the determination of the thermal transpiration effect were within one per cent accuracy, the overall accuracy of this test was approximately the same as for the permeability test.

CHAPTER V

DISCUSSION OF EXPERIMENTAL RESULTS

Equilibrium Vapor Pressure

Introduction

In order to accurately predict freeze-drying rates, it is important to know the equilibrium vapor pressure of the product being dried. During freeze-drying, a dried layer develops which is distinctly separate from the frozen wet layer. In analytical calculations of freeze-drying rates, a boundary condition generally used is that the temperature of the interface separating the dried and undried regions is equal to the equilibrium temperature of pure ice at a pressure equal to that which exists at the interface. Recent calculations by the author for freeze-drying of beef show that errors of ±2 °C in the assumed interface temperature can cause an error of 100 per cent in the calculated heat flux through the undried layer. Consequently, it is desirable to know as accurately as possible the equilibrium vapor pressure-temperature relationship for frozen meat.

Bovine muscle consists essentially of a liquid phase dispersed throughout a solid matrix. The liquid phase is an aqueous solution which contains dissolved salts and proteins. When the meat is frozen, it might well be expected that the thermodynamic properties of the frozen liquid phase would be different from those of ice. In particular, the equilibrium vapor pressure of the frozen liquid in the meat might be expected to deviate from that of pure ice. The present study

of the equilibrium vapor pressure of beef steak has been prompted by these considerations.

Results for round, sirloin, and T-bone steak are summarized graphically in Figure 5. The points shown represent runs for both ascending and descending temperatures. Since there is no evidence of hysteresis, it is concluded that the pressures measured are equilibrium values. The legend in this figure indicates the various grades of beef used. Some results are also presented for a sample which was freeze-dried for several hours before the clamp on the vacuum line to the pump was closed. This sample was completely surrounded by a thin layer of dried meat.

Mechanism of Vapor Pressure Depression

The experimental results consist essentially of two parts: vapor pressure data for frozen bovine muscle itself and data for the frozen liquid squeezed from the muscle. From Figure 5, it is clear that the vapor pressure is depressed below that of pure ice at the same temperature, and that the depression is larger for the frozen meat than for the meat juice.

In discussing these results, we shall consider a piece of meat to consist of a frozen liquid phase which is dispersed throughout a solid matrix. This matrix may contain cavities and capillaries. The liquid phase, frozen meat juice, is a dilute aqueous solution containing dissolved proteins and salts. The equilibrium vapor pressure of meat is a function of the nature of the frozen liquid phase, of the solid matrix, and of the interactions between these two. In interpreting the difference between the equilibrium vapor pressure of frozen meat and

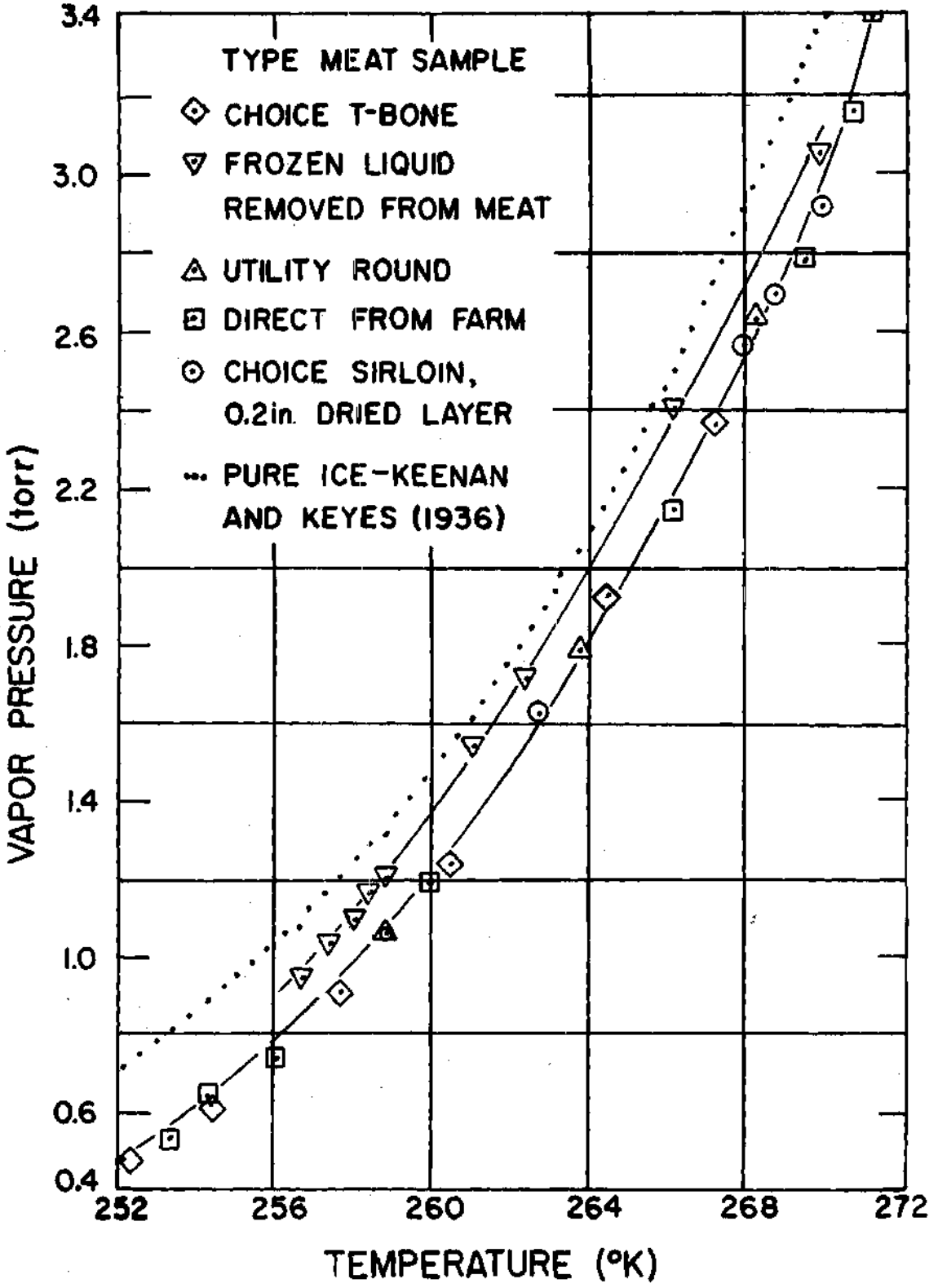

Figure 5. Equilibrium Vapor Pressure.

pure ice at the same temperature, three possible contributing factors will be considered.

1. The influence of the concentration of solute species in the frozen liquid.

2. The influence of concave interfaces between the vapor phase and the frozen liquid phase.

3. The restriction of the maximum possible size of crystals of the frozen substance by the solid matrix.

Consider first the effect of dissolved solute species in the frozen phase. If the latter is an ideal solid solution, then Raoult's Law as given by Lewis and Randall (29) will apply.

$$\bar{P}_w / \bar{P}_w^o = 1 - y \tag{5.1}$$

Where $\bar{P}_w$ is the partial pressure of water above the solid solution, $\bar{P}_w^o$ is the vapor pressure of pure ice at the same temperature, and y is the total mole fraction of all solute species in the solid solution. Since the solute consists of a number of (unknown) components,

$$y = \sum_i y_i \tag{5.2}$$

where y_i is the mole fraction of solute species i. Thus,

$$\bar{P}_w / \bar{P}_w^o = 1 - \sum_i y_i \tag{5.3}$$

Clearly, the greater the total concentration of solute species present in the frozen liquid phase, the lower will be the vapor pressure of

water compared to that of pure ice at the same temperature. Of course, equation 5.3 is an oversimplification, since Raoult's Law is valid only for ideal solutions, and in view of the electrolytic nature of the frozen liquid phase in meat, deviations are certainly to be expected. Nevertheless, equation 5.3 should serve to account for the influence of dissolved solute species to a degree of approximation sufficient for our purpose. A more accurate treatment of the solid solution behavior would require knowledge of the chemical and physical constitution of meat that we do not possess.

The second effect has its origin in the influence of the curvature of a surface on the vapor pressure. Consider two surfaces, one planar and the other with a concave indentation of radius r_c. The molecules at the surface in the latter case are surrounded by more nearest neighbors than are the molecules at the planar surface. This is the molecular basis for the fact that the energy required to generate a unit area of fresh surface is less for a concave than for a planar surface. The surface free energy and the vapor pressure are accordingly lower for a concave surface. This result can be expressed thermodynamically by the Gibbs-Kelvin equation which is presented in many references such as Swalin (30),

$$\tilde{R}_g T[\ln(P_r/P_\infty] = -2e_s\tilde{V}/r_c \qquad (5.4)$$

where P_r and P_∞ refer to the vapor pressures above the concave and planar surfaces, respectively; e_s is the surface free energy of the solid in equilibrium with its vapor; $\tilde{V}$ is the partial molar volume of the volatile substance; and $\tilde{R}_g$ is the universal gas constant of

the volatile substance. Thus if the surface of a piece of beef muscle contains many concave indentations, the equilibrium vapor pressure will be lowered to an extent given by equation 5.4. Such concave indentations could exist at the openings of capillary-like channels in the meat.

The third effect mentioned above is suggested by the possibility of the existence in the meat matrix of cavities which might by their size limit the extent to which ice crystals could grow. If the maximum size of the crystals is restricted to a small value in this manner, then the ratio of the surface area to the volume of these crystals would be large. This would in turn give rise to a surface free energy which would be <u>higher</u> than the surface free energy at a planar surface. This would in turn increase the vapor pressure of the water because at equilibrium, the chemical potential must be uniform throughout the system.

To summarize, effects 1 and 2 would tend to cause a decrease in the equilibrium vapor pressure, while effect 3 would tend to increase it. We now proceed to estimate the magnitude of these effects.

Consider first the effect of concave surfaces, effect 2. A capillary radius of 0.075 mm is suggested by the data of Luyet (3). Weast (31) gives a value for the surface free energy of 77 ergs/cm^2. Using these values in equation 5.4, the calculated vapor pressure depression turns out to be less than 0.01 per cent.

Regarding effect 3, we note that if the capillary radius of 0.075 mm is also characteristic of the internal cavity size (as seems to be the case), then the increase in the vapor pressure due to the restriction of the size of crystals of ice will also be of the

order of 0.01 per cent.

We thus see that the magnitude of effects 2 and 3 are both negligible compared to the observed vapor pressure depressions.

We accordingly conclude that the lowering of the vapor pressure is due to the formation of a solid solution in the frozen liquid phase by dissolved solute species and ice. This conclusion immediately raises the question of why the vapor pressure of the frozen beef muscle is depressed more than that of the frozen meat juice. To answer this question we shall use Figure 6, in which we depict an idealized model of meat which we shall use to interpret the vapor pressure data. The model depicted is essentially that of a cross-linked ionic network which is pervaded by an aqueous solution. The latter contains dissolved ionic species, and perhaps electrically neutral protein molecules. These solute species are mobile at temperatures above the freezing point. In addition to these solute species, however, there are also ions which are chemically bound to the polymer chains of the network, and there are other hydrophilic groups on these chains. As long as the aqueous phase remains inside the network, both these immobile ions and hydrophilic groups are able to act as solute species. However, when the aqueous phase is squeezed out of the network, only the mobile solute species are removed; those solute species that are permanently attached to the network chains necessarily remain behind. Therefore, the total concentration of solute species in the meat juice which is removed is less than the concentration present in the meat itself. It is for this reason that the vapor pressure of the frozen meat juice is higher than that of frozen meat. These ideas can be put on a quantitative basis

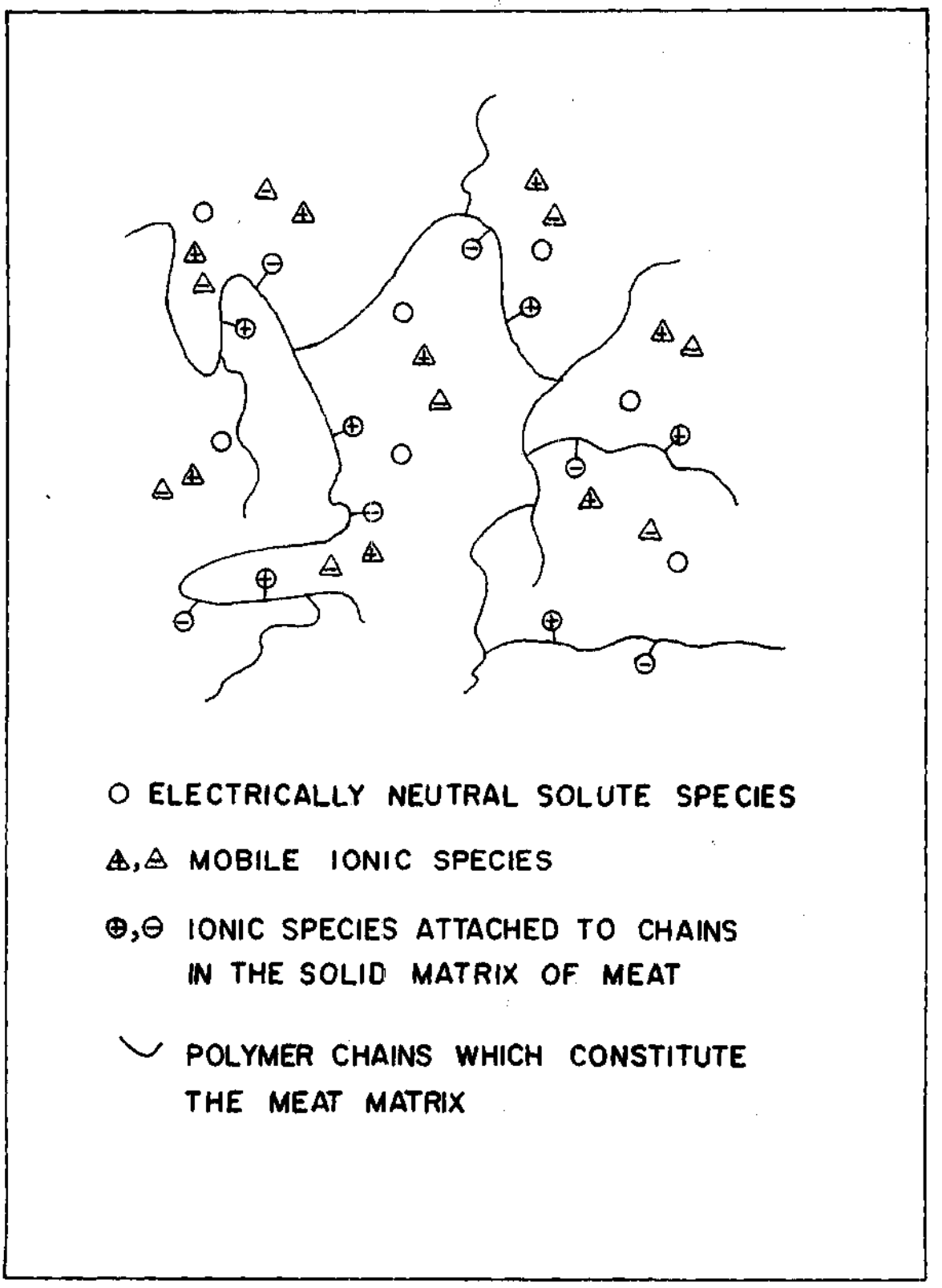

Figure 6. Idealized Model of Meat.

through use of equation 5.3. The results of such calculations are to be found in Table 1, where we tabulate the values y, the total mole fraction of solute species in the aqueous phase when the latter is inside the meat, and after it has been squeezed out. The variation of these calculated mole fractions with temperature is primarily due to the oversimplification that is introduced by the assumption of ideal solution behavior. The fourth column of Table 1 shows the increment in solute concentration between the frozen meat juice and the frozen meat itself.

Table 1. Mole Fraction of Solute Species in the Solid Solution

T(°K)	y_s	y_{Ls}	$y_s - y_{Ls}$
252.8	0.32	0.13	0.19
255.5	0.27	0.11	0.16
258.3	0.19	0.11	0.08
261.1	0.18	0.09	0.09
263.9	0.15	0.09	0.06
266.7	0.14	0.06	0.08
269.4	0.15	0.05	0.10

y_s - total mole fraction of solute species in the aqueous phase when the latter is in the meat

y_{Ls} - total mole fraction of solute species in the aqueous phase after the latter has been squeezed out

Additional confirmation of our model of frozen meat can be obtained by examining the temperature dependence of the vapor pressure data. These data are plotted in the customary manner in Figure 7, as ln p vs. 1/T. To interpret the slopes of the lines we use a variant of the Clausius-Clapeyron equation,

$$\frac{d \ln \overline{P}}{d \frac{1}{T}} = - \Delta\tilde{H} / \tilde{R} \qquad (5.5)$$

where

$$\Delta\tilde{H} = \Delta\tilde{H}_{SUB} - \Delta\tilde{H}_{M} \qquad (5.6)$$

$\Delta\tilde{H}$ - molar heat of sublimation of ice

$\Delta\tilde{H}_{M}$ - change in enthalpy occurring when one mole of ice is transferred to a solid solution over which the partial pressure is $\overline{P}$.

For convenience, we shall call $\Delta\tilde{H}_{M}$ the "heat of mixing." From the slopes of the lines in Figure 7, and using a value of $\Delta\tilde{H}_{SUB}$ of 12,200 cal/mole given by Keenan and Keyes (28), we find that

$$\Delta\tilde{H}_{M} = -2680 \text{ cal/mole for frozen bovine muscle}$$

and

$$\Delta\tilde{H}_{M} = -1030 \text{ cal/mole for frozen meat juice.}$$

The negative signs signify that the formation of the solid solution from ice and solute species is an exothermic process. The magnitudes indicate that considerably more heat is liberated in the formation of the solid solution in meat itself than in meat juice. In fact, the

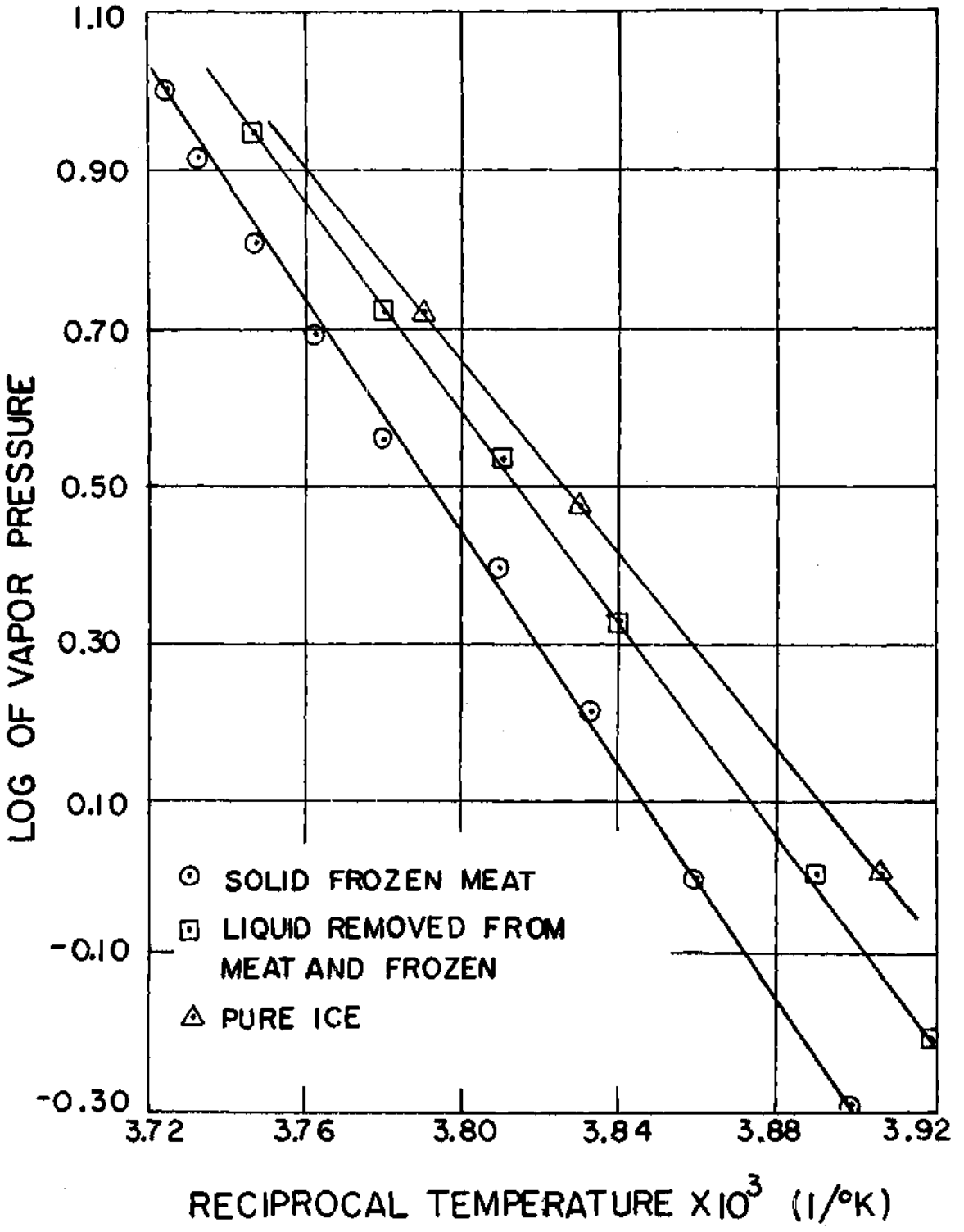

Figure 7. Vapor Pressure vs. Reciprocal Temperature for Meat and Meat Juices.

enthalpy change for the process:

$$1 \text{ mole } H_2O \text{ in meat juice} \rightarrow 1 \text{ mole } H_2O \text{ in meat}$$

is $\Delta H' = -2680$ cal/mole - (-1030 cal/mole) = -1650 cal/mole. These values are quite compatable with our ionic network model for meat. The excess enthalpy $\Delta H' = -1650$ cal/mole represents, according to this model, the additional heat of hydration of ions and hydrophilic chain groups that occurs per mole of water when the water is inside the meat matrix.

The foregoing analysis of the vapor pressure data assumes that the pressures measured were true equilibrium values. Effects due to the rate of transfer of water through membrane materials in the meat have not been deemed significant. Partial justification for this simplification is to be found in the lack of hysteresis in the observed pressure-temperature relationships.

Using Figure 7, an empirical equation can be obtained for the equilibrium vapor pressure as a function of temperature for beef. Using the equation for a straight line gives

$$\bar{p}_w = \exp(27.70 - 12900.0/T) \qquad (5.7)$$

where T is in °R and p in torr.

Permeability Coefficient

Effect of Thickness

The derivation shown in Appendix B shows that the permeability defined by

$$\varepsilon(p_m) = -\mu W_w L/\rho \, \Delta p$$

should be a function of pressure only for a given sample and temperature. Typical experimental results which are shown in Figure 8 for four samples of different lengths show that this is not the case for the measurements made. The samples were cut from the same piece of round steak and freeze-dried under the same conditions. This figure shows that the permeability is definitely a function of the thickness. Entrance and exit losses due to the sudden contraction and expansion of the gas as it moves through the porous sample and the effect of a developing velocity profile at the capillary entrance cause a pressure drop which is independent of the sample thickness. Thus, from the definition of permeability it is seen that these effects would cause the permeability to be thickness dependent. However, calculation by the author show that these effects have a negligible influence on the permeability of beef under the conditions stated. A plausible cause for the thickness dependence of the permeability is "crimping" at the ends of the capillaries due to cutting the sample. This restriction of the capillary ends would reduce the mass flow by an amount which is only a function of average pressure and the total pressure gradient and not length since the crimping occurs at both ends independently of the sample thickness. Accounting for the decreased flow due to crimping, equation B.32 becomes

$$W' = -\left[1 - \exp(-2r_c/\lambda)\right]\left[\frac{B_4 \Delta p \rho}{\mu L}\left(1 + \frac{B_5}{p_m}\right)\right] + B_3 \frac{\Delta p}{L} \exp(-2r_c/\lambda) - k(p_m, \Delta p) \qquad (5.9)$$

where $k(p_m, \Delta p)$ represents the influence of crimping and depends on the mean pressure and the pressure drop across the sample. An overall permeability which includes the crimping effects will be defined analogously

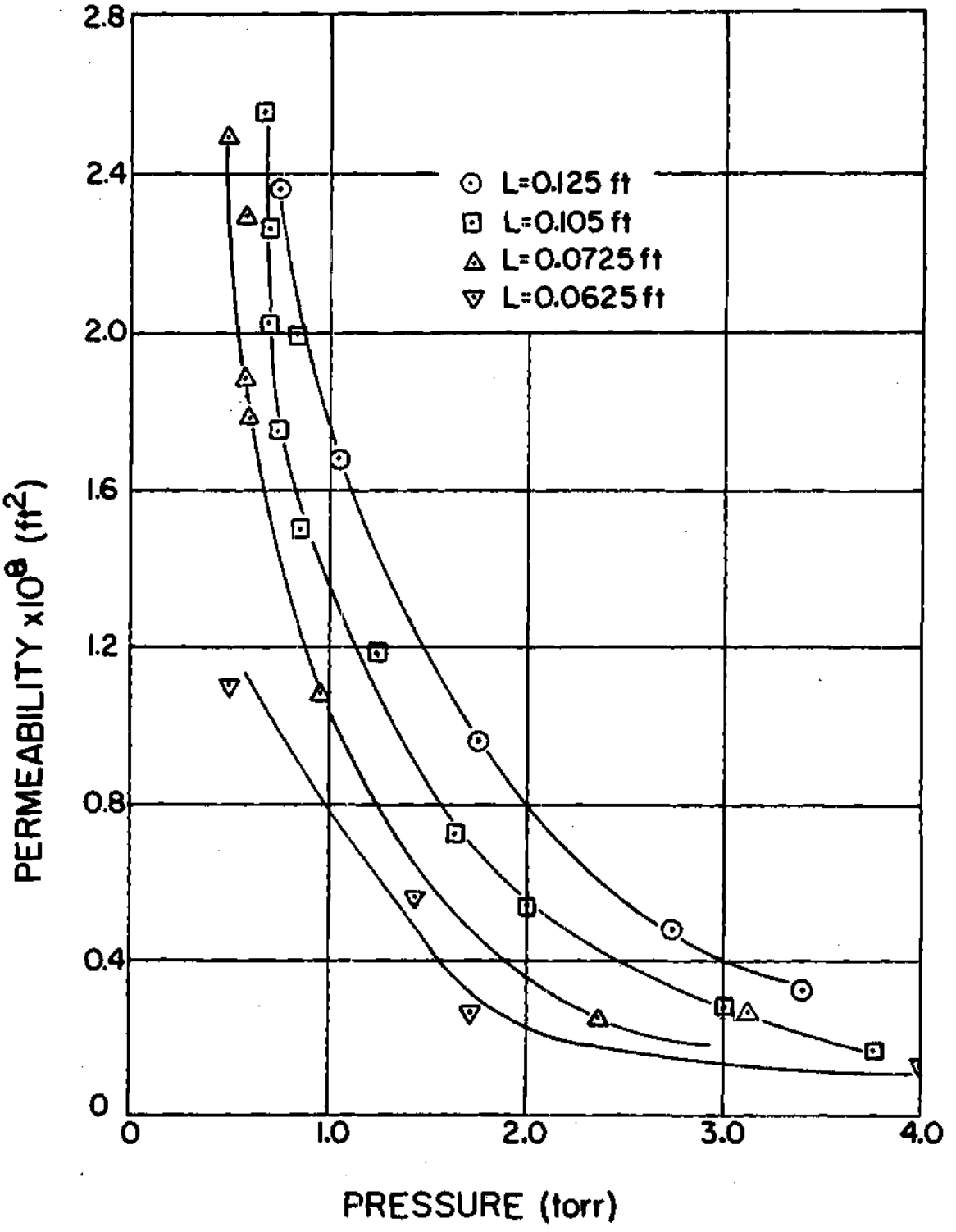

Figure 8. Permeability vs. Pressure with Length as a Parameter.

to $\varepsilon(p_m)$ by

$$\varepsilon' = \mu W' L/\rho\Delta p$$

Substituting equation 5.9 into 5.10 and using equation 5.8 gives

$$\varepsilon' = \varepsilon(p_m) - \frac{\mu L_c}{\rho\Delta p} k(p_m,\Delta p)$$

Note that $\mu L\ k(p_m,\Delta p)/\rho\Delta p$ represents the contribution to the overall permeability ε' due to crimping and could be a function of average pressure, pressure drop, sample thickness, and temperature. Thus for a sample with no crimping $\mu L\ k(p_m,\Delta p)/\rho\Delta p = 0$.

In order to show the effect of thickness on the permeability, a plot of overall permeability ε' versus thickness for various pressures is given in Figure 9. All data shown are for a constant temperature of 77°F. Mathematically, the slope of this plot represents

$$\varepsilon'_L = \left.\frac{\partial\varepsilon'}{\partial L}\right|_{p_m,T,\Delta p} + \left(\left.\frac{\partial\varepsilon'}{\partial\Delta p}\right|_{p_m,T,L}\right)\frac{d\Delta p}{dL}$$

where ε'_L is defined by $\left.\frac{\partial\varepsilon'}{\partial L}\right|_{p_m,T}$.

A useful result is obtained by plotting ε'_L versus p_m. This plot is shown in Figure 10 and demonstrates that ε'_L is approximately a function of average pressure only for a given sample and temperature. Thus, regardless of the sample thickness or total pressure gradient ε' can be calculated from

$$\varepsilon' = \varepsilon'_L L + \text{Constant} \qquad (5.13)$$

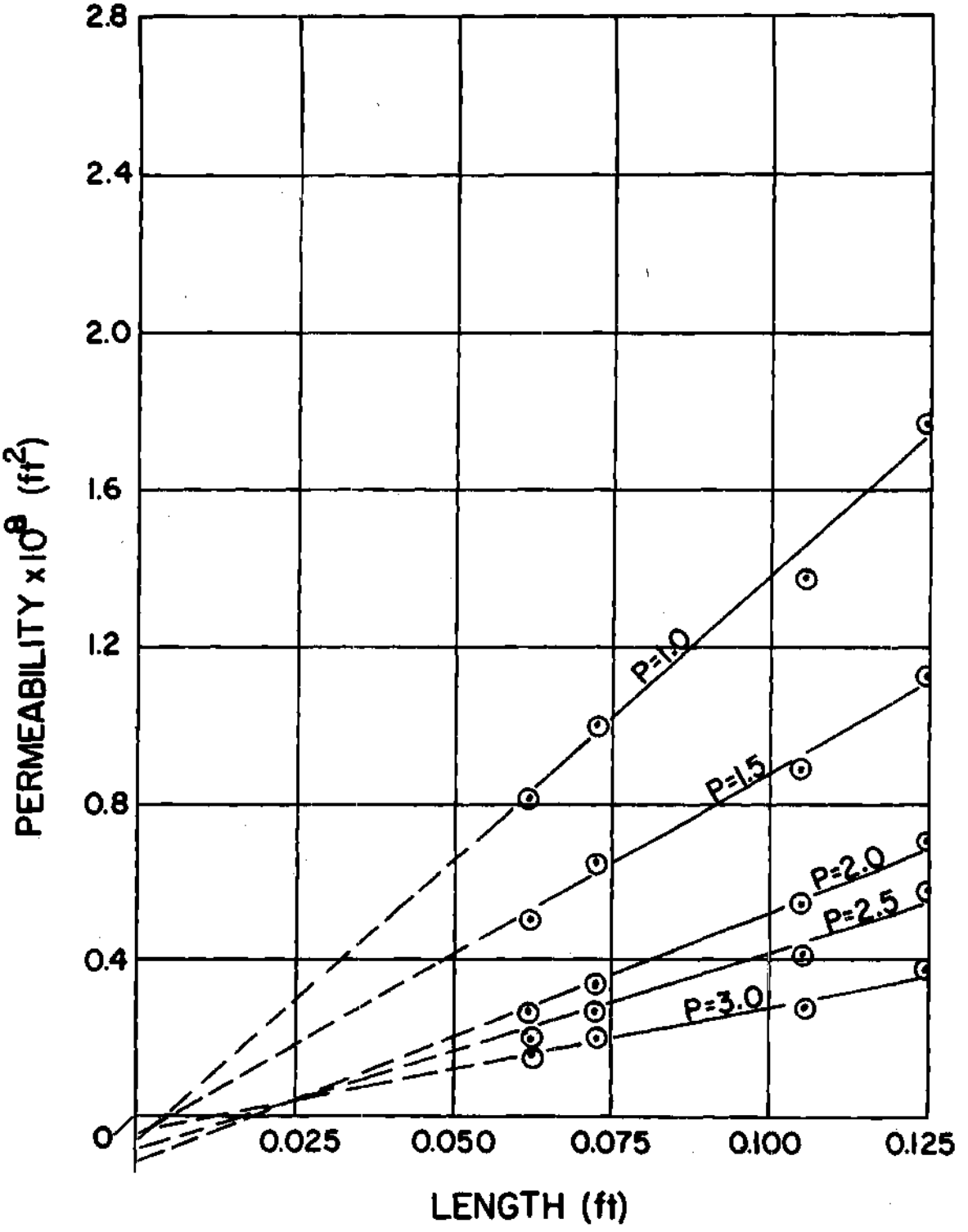

Figure 9. Permeability vs. Length with Pressure (torr) as a Parameter.

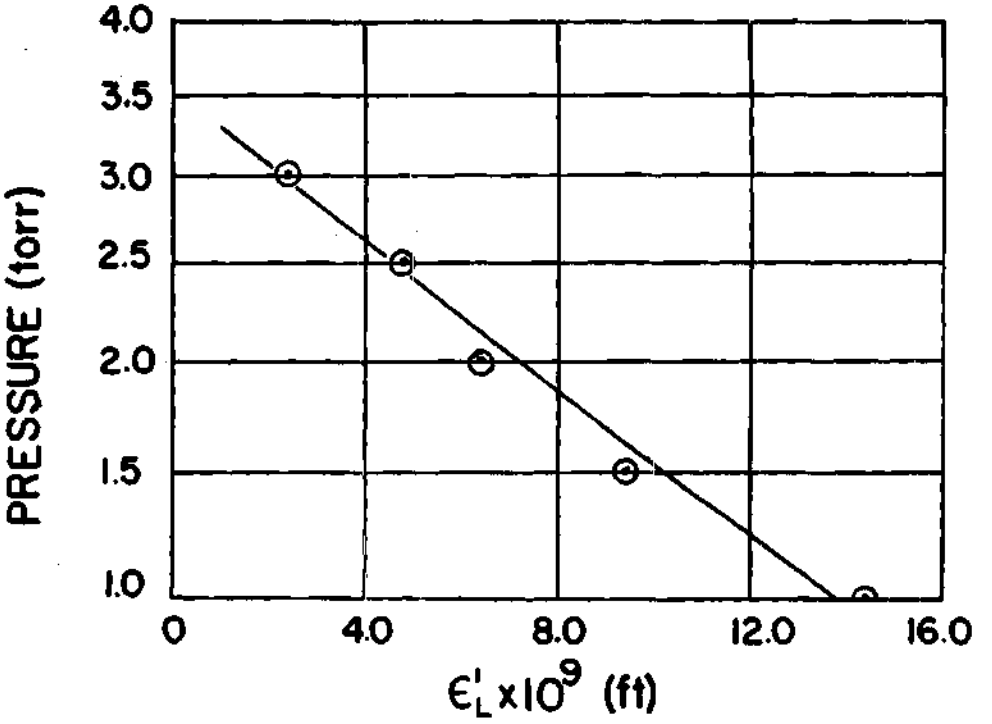

Figure 10. ε'_L Versus Pressure.

Noting from Figure 9 that $\varepsilon' \approx 0$ at $L = 0$ and substituting the equation for ε'_L obtained from Figure 10 into equation 5.13 gives

$$\varepsilon' \approx L(10)^{-8}(13.5 - 10.8 \ln p_m) \qquad (5.14)$$

where L is in feet, p in torr, and ε' in ft^2. Note that this result is valid for a temperature of 77 °F. ε' can be modified for other temperatures as shown in the next section.

Equation 5.14 is valid for the thickness effect of permeability when both ends of the capillaries are crimped. In the actual freeze-drying situation only one end of the capillaries is crimped so that the thickness effect is only one half of that used in equation 5.14.

Consequently, an equation which can be used to predict permeability for the actual freeze-drying case is given by

$$\varepsilon' \approx \frac{1}{2} L\, 10^{-8}(13.5 - 10.8 \ln p_m) \qquad (5.16)$$

Effect of Temperature

Values for the permeability coefficient reported in this thesis are for an average temperature of approximately 77 °F. For the freeze-drying situation the average temperature will be some what less; and, consequently, it is desirable to be able to calculate the effect of average temperature on the permeability coefficient. The following procedure can be used to calculate the correction for temperature.

For the Temperature at Which the Data was Taken.

(1) Calculate μ from the equation given in (32)

$$\mu = .17(10)^{-6}T^{1.116}$$

where μ is in poise and T in °K.

(2) Assuming diffuse reflections use the definition of B_5 and the calculated value of μ to obtain the value of B_5.

(3) Calculate λ using the equation given in (33).

$$\lambda = (68.8)10^{-3}/P$$

where λ is in mm and p in torr.

(4) Calculate the magnitude of $F(r_c/\lambda)$ from its definition using the value of λ obtained in step 3 and $r_c = 0.075$ mm as given by Luyet (3).

(5) Calculate B_3 from its definition.

(6) Assuming that $\Gamma/\tau \approx \frac{1}{L}$ calculate B_4 from its definition. Note that B_4 is not temperature dependent.

(7) Use the experimentally determined values of ε', the values of B_3, B_4, B_5, $F(r_c/\lambda)$ obtained in steps 1 through 6, and the sample dimensions to calculate $\mu Lk(p_m,\Delta p)/\rho\Delta p$ from equation B.26.

(8) Calculate $k(p_m,\Delta p)$ from the value of $\mu Lk(p_m,\Delta p)/\rho\Delta p$ calculated in step 7.

For the Temperature for Which the Permeability is Desired

(9) Calculate μ from

$$\mu = (.17)10^{-6}T^{1.116}$$

(10) Calculate B_5 from its definition using the value of μ obtained in step 9.

(11) Calculate B_3 from its definition.

(12) Using the value of B_4 obtained in step 6 and the values of $F(r_c/\lambda)$ obtained in step 4 and the magnitude of $k(p_m,\Delta p)$ found in step 8, the values of B_5 and B_3 obtained in steps 10 and 11, and the value of μ obtained in step 9, calculate ε' for the desired temperature from equation 5.11.

Variation with Different Samples

The complete data for samples of different grades and cuts of beef steak frozen and dried at different rates are given in Appendix C. Comparison of the data for the entire range of sample tested accounting for the length dependence of the permeability shows a permeability variation of approximately 10 per cent. This variation is due to the different pore size and arrangement which exists in the samples considered. In addition to the differences in physical make up of the grades and cuts of samples considered, the non-uniformity of pore structure is due

to the different rates used in the initial freezing of the sample. This latter effect is described in reference (3).

Thermal Transpiration Effect

Kennard (8) shows that for the region between viscous and molecular flow that a positive temperature gradient along the axis of a tube through which a gas flows will produce an increased flow rate over that of the isothermal flow. The equation for the case of non-uniform temperature is

$$W_w = \frac{\Pi}{8} \frac{r_c^4 p}{\mu RT} \left(1 + 4 \frac{\xi}{r_c}\right) \frac{dp}{dx} + \frac{3}{4} \Pi \frac{\mu r_c^2}{T} \frac{dT}{dx} \qquad (5.17)$$

$$\text{where } \xi = \frac{2-s}{s} \frac{\Pi}{2} \frac{\mu}{2} RT$$

The terms on the right side of equation 5.17 represent respectively the contributions to the mass flow due to a total pressure and temperature gradient.

Since the temperature gradients in freeze-drying work are relatively steep, it is desirable to ascertain whether the flow due to the temperature gradient can be neglected. The additional mass flow due to thermal transpiration for a positive temperature gradient should increase the permeability as defined by equation 5.10. Experimental data for calculation of the permeability were obtained for flow through a given sample with and without a temperature gradient. These data are plotted in Figure 11 and show that the transpiration effect is negligible in comparison to hydrodynamic flow. Note that experimentally a negative temperature gradient was used which theoretically should decrease the permeability.

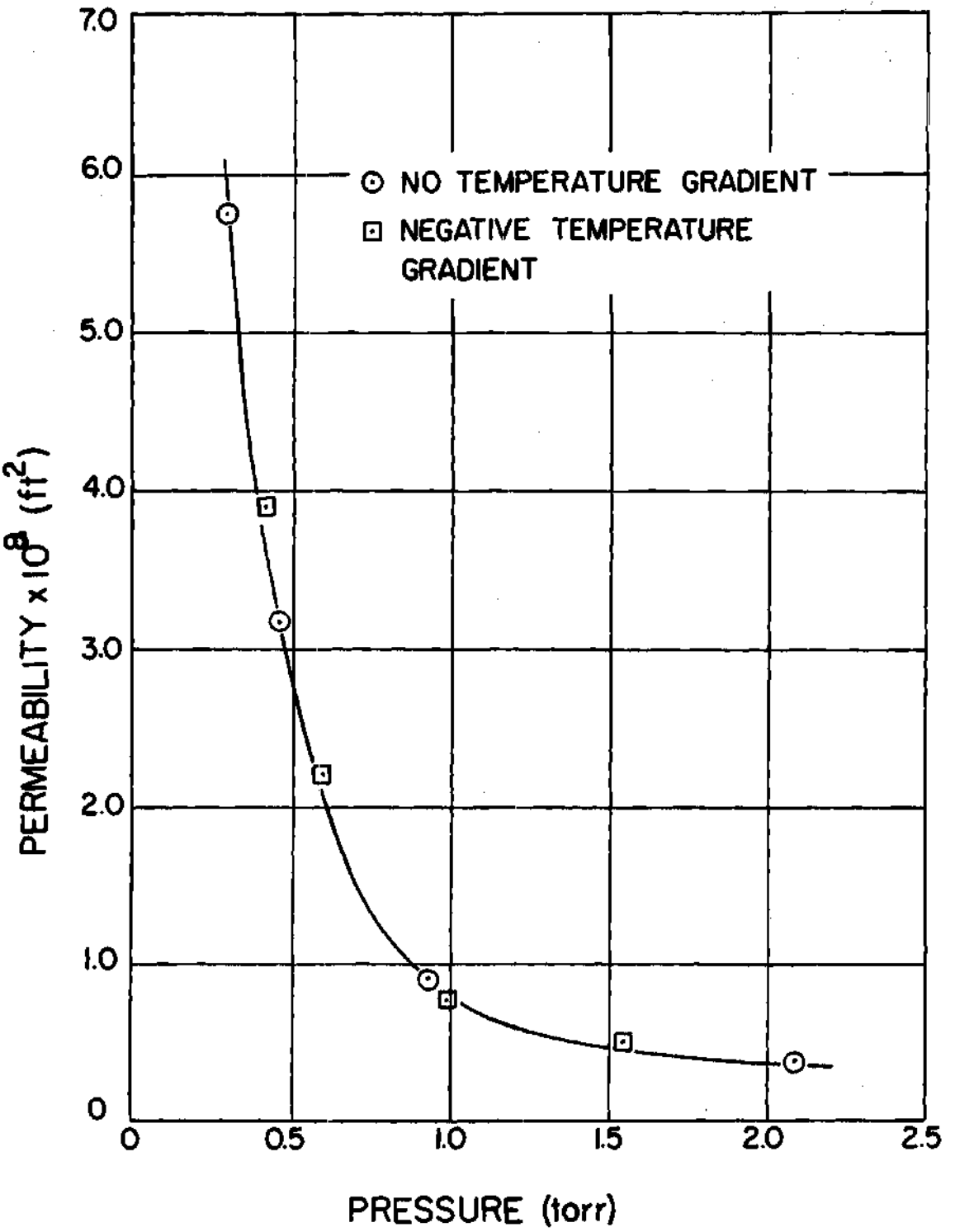

Figure 11. Effect of Thermal Transpiration on Permeability.

Confirmation of the experimental finding is obtained through calculation of the ratio of the transpiration flow to hydrodynamic flow from equation 5.17. This calculation shows that for the pressure range considered the ratio is less than 0.03.

CHAPTER VI

DISCUSSION OF ANALYTICAL RESULTS

Analytical Results of Chapter II

Typical Results from Analytical Equations for Drying Rate

The analytical equations for drying rate for cases 1 and 2 as derived in chapter II were solved with the aid of a digital computer. Pressures of 1, 2, and 3 torr were considered, and the following values of effective thermal conductivity (16) for the dried region (Region I) were used respectively: .026 B/ft-hr-°R, 0.028 B/ft-hr-°R, and 0.029 B/ft-hr-°R. A value of 0.6 B/hr ft-°R as suggested by Miller (34) was used for the frozen layer thermal conductivity and the thermal diffusivity of the dried layer was taken as 0.06 ft^2/hr. All calculations were for a sample .125 feet thick. The interface position as a function of time obtained from these calculations is shown in Figure 12. The boundary conditions used are given in the Figure 12.

The results shown in Figure 12 indicate three important observations:

(1) The exact solution (case 1) and quasi-steady solution case 2 with the same boundary conditions yield almost identical results. Consequently, the quasi-steady solution is sufficient for drying rates of the order considered in the calculations.

(2) The drying rate decreases slightly with decreasing pressure for the pressure range 1 to 3 torr. Hardin (18) and Hatcher (21) have observed this fact experimentally. It is to be expected that the

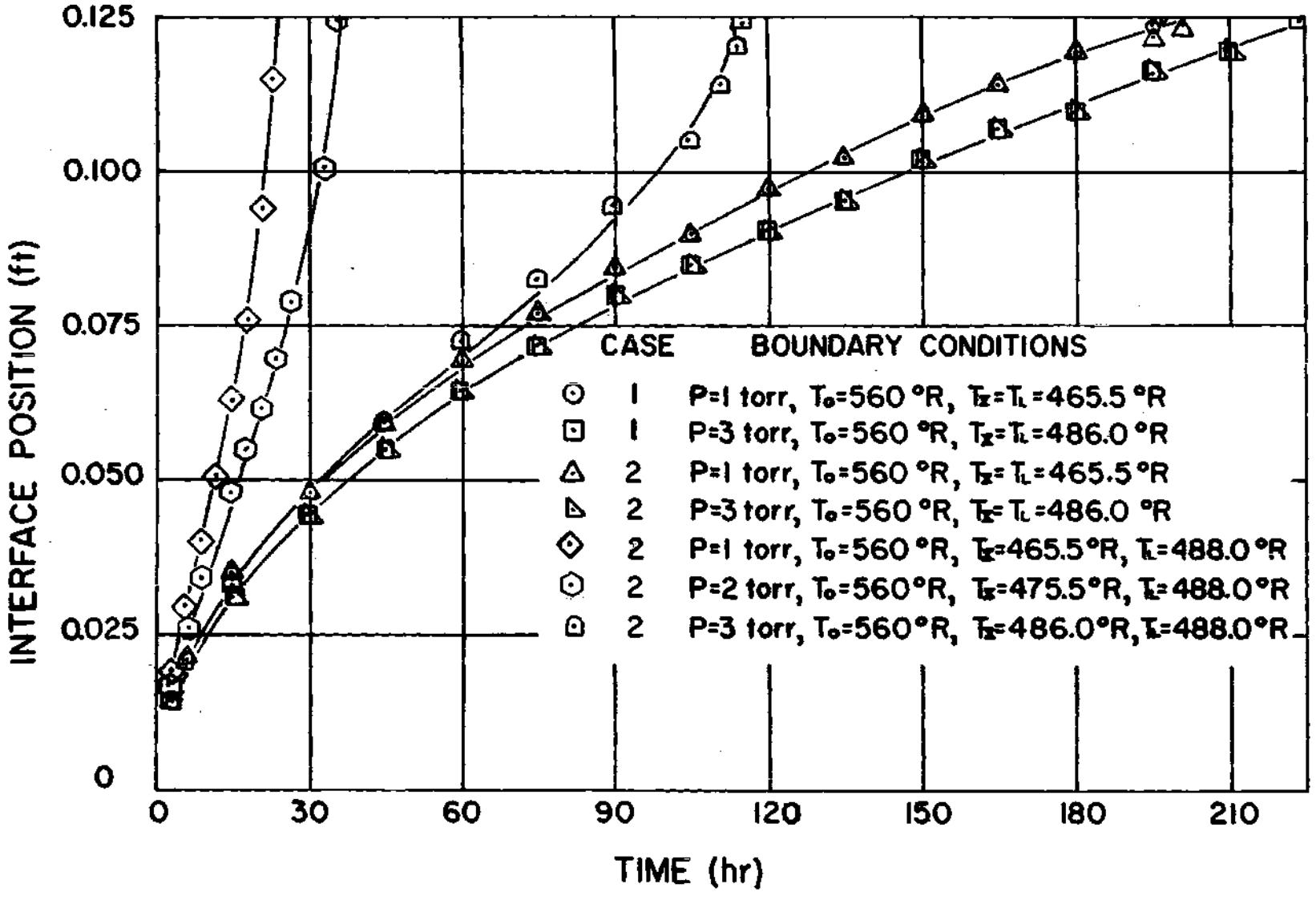

Figure 12. Interface Position Versus Time for Case 1 and Case 2.

decrease in drying time with pressure would cease at a pressure level sufficiently low that the volume flow rate is in excess of the capacity of the porous dried layer.

(3) Back face heating (heat input from face at X = L) can tremendously reduce the time required for freeze-drying. Figure 12 shows that for the same pressure back face heating reduces the drying time by approximately 70 per cent. This result is due to the fact that the thermal conductivity of the frozen layer is approximately 20 times that of the dried layer. Note, however, that a method must be obtained for eliminating drying from the back face. If drying occurs on the back face the effective thermal conductivity of the frozen layer will decrease greatly. This conclusion is also discussed by Hardin (18).

Selection of Appropriate Boundary Conditions

The following method was used in determining appropriate boundary conditions in calculating the results for Chapter II:

At the Position x = 0

This temperature should be set as high as the food product can withstand without damaging the quality of the product. For beef a temperature of 100 °F is admissible.

At the Position x = X

This temperature has been found by experiment for a pressure greater than 0.5 torr and concentration of water nearly 1 to be set by the chamber pressure in the following manner. The temperature corresponds to the saturation temperature of the subliming phase of the food product at the chamber pressure. Thus, the data obtained for the vapor pressure of beef steak (see page 52) is very useful in analyzing

the freeze-drying process of this food product since for the analytical calculations one can decide on the chamber pressure and then immediately determine the interface temperature from Figure 5.

At the Position x = L

This temperature should be maintained just under the melting temperature of the frozen meat which would be approximately 30 °F.

Analytical Results of Chapter III

Effective Average Diffusion Coefficient

The experimental results for $(D_t)_e$ from measurements made on several samples of beef are given in Table 2. In addition, the values of $(D_t)_e$ calculated by using the theory presented in Chapter III are given for each of the conditions used in the experimental work. In applying the theory, a value for $(D_{12})_e$ of 1/3 the value for free diffusion in air at atmospheric pressure as suggested by Harper and Chichester (17) was used. It is seen that close agreement exists between these theoretical and experimental values of $(D_t)_e$ appearing in Table 2. Since different samples were used, the property variation of the samples can account for most of the deviation between theory and experiment.

The final information presented in Table 2 is the value of $(D_t)_e$ predicted by the theory given in reference 17. A much wider discrepancy exists between this theory and the experimental data than exists for the analytical work of Chapter III. This lack of correlation probably lies in the assumption of reference (17) that the transfer modes of heat conduction and diffusion are analogous. As discussed in the introduction of Chapter III, these modes are not analogous; as a consequence, a large variation from experiment is to be expected.

Table 2. Effective Average Diffusion Coefficient

Average Pressure (torr)	$(D_t)_e$ Obtained Experimentally (ft^2/sec)	$(D_t)_e$ Obtained by Theory of Chapter III (ft^2/sec)	$(D_t)_e$ Calculated by Theory of Reference(17) (ft^2/sec)
1.44	.015	.017	.031
1.58	.019	.018	.028
1.64	.012	.015	.028
2.25	.010	.010	.021
2.28	.017	.015	.020

Typical Results from Analytical Equations for Drying Rates

The equations for the drying time given in Chapter III for the cases of back face drying were solved with the aid of a digital computer using the method outlined on page 32. In addition equations 3.44 and 3.46 for the case of no back face heating were solved simultaneously with the aid of a digital computer. Total chamber pressures of 1.0, 2.0, and 3.0 torr were considered with water-vapor partial pressures in the chamber of 50 to 60 per cent of the total pressure. The thermal conductivities used were the same as used in the computation of the results for Chapter II (see page 72). All calculations are for a sample thickness of .125 feet. Values of (D_{te}) estimated from the data given in Table 2 of .017, .013, .011 $\frac{ft^2}{sec}$ corresponding to chamber pressures of 1, 2, and 3 torr were used. For chamber pressures of 1, 2, and 3 torr the following values of $\tilde{\varepsilon}$ estimated from Appendix C were used respectively: -0.00112, -0.0094, and -0.00085 $\frac{\text{mole ft}}{\text{lbf hr}}$.

Using the results obtained from the equations of Chapter III, a plot of interface position versus time is shown in Figure 13 for the conditions on the graph. Note that the condition of heating from the back face is considered. The figure shows that the drying time increases with increasing water-vapor concentration. Similar results were obtained from the special case of no back face heating. The complete results from the computer are given in Appendix D.

To understand the reason for the decreased drying rate consider a sample drying at a constant chamber pressure of 1 torr and face temperature T_0 of 560 °R. Let the initial partial pressure of the water-vapor in the chamber be 0.5 torr and look at the result of suddenly increasing this partial pressure to 0.6 torr. Since this decreases the concentration gradient between the interface and chamber the flow as given by equation 3.16 will decrease. The accumulation of water-vapor at the interface will increase the partial pressure of the water-vapor and the temperature at the interface. Thus the concentration gradient will be increased and the mass flow will increase but not to its initial level since the temperature gradient and energy input have decreased. Consequently, a new steady state condition of a smaller energy input and mass flow rate will be achieved.

Interface Temperature

A plot of interface temperature versus interface position for a total pressure of 2 torr and water-vapor partial pressures of 1.0 and 1.2 torr is shown in Figure 14. Curves are shown with and without back face heating. Note that the analytical equations show the interface temperature to be constant when there is no energy input from the

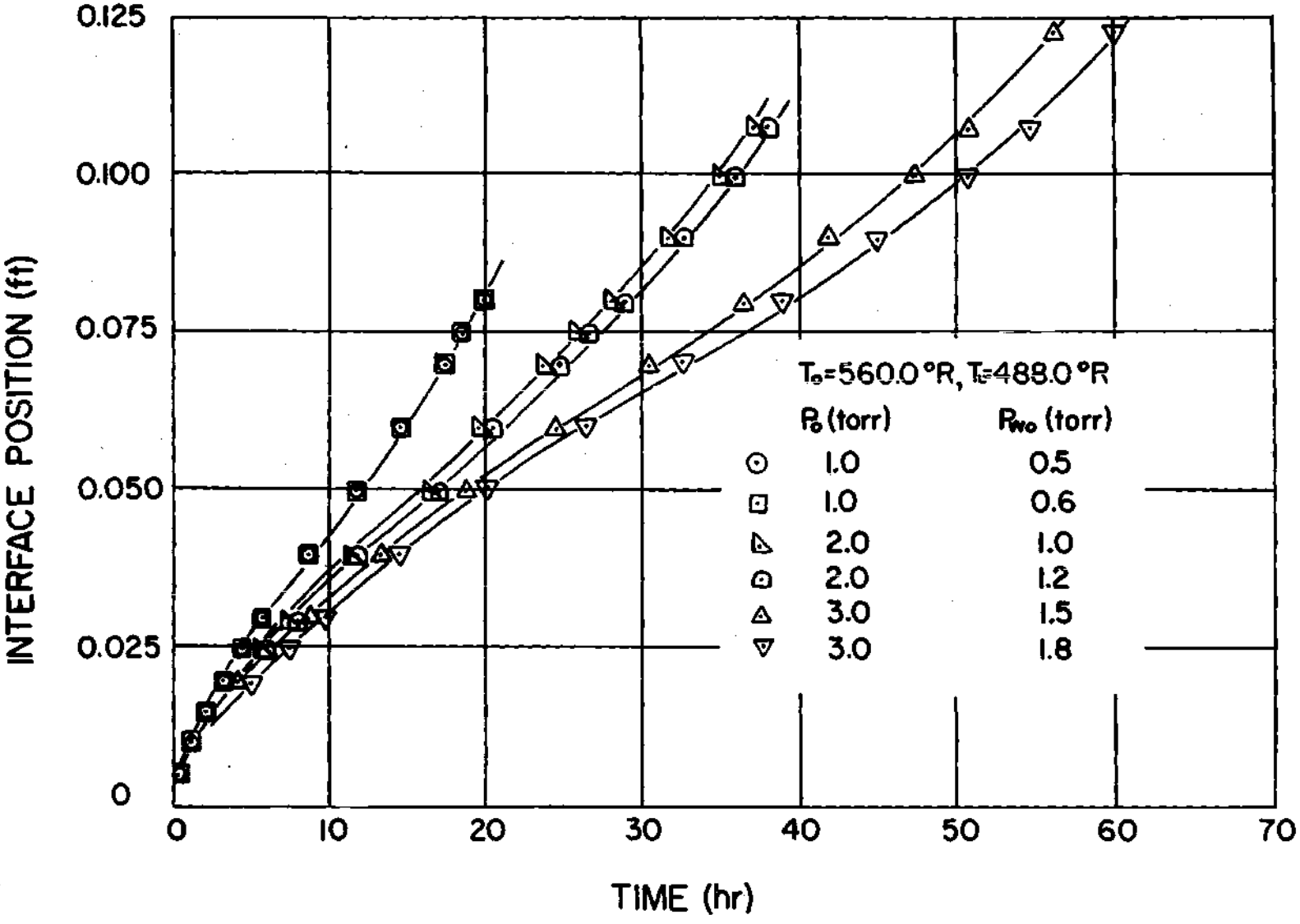

Figure 13. Interface Position vs. Time for Results of Chapter III.

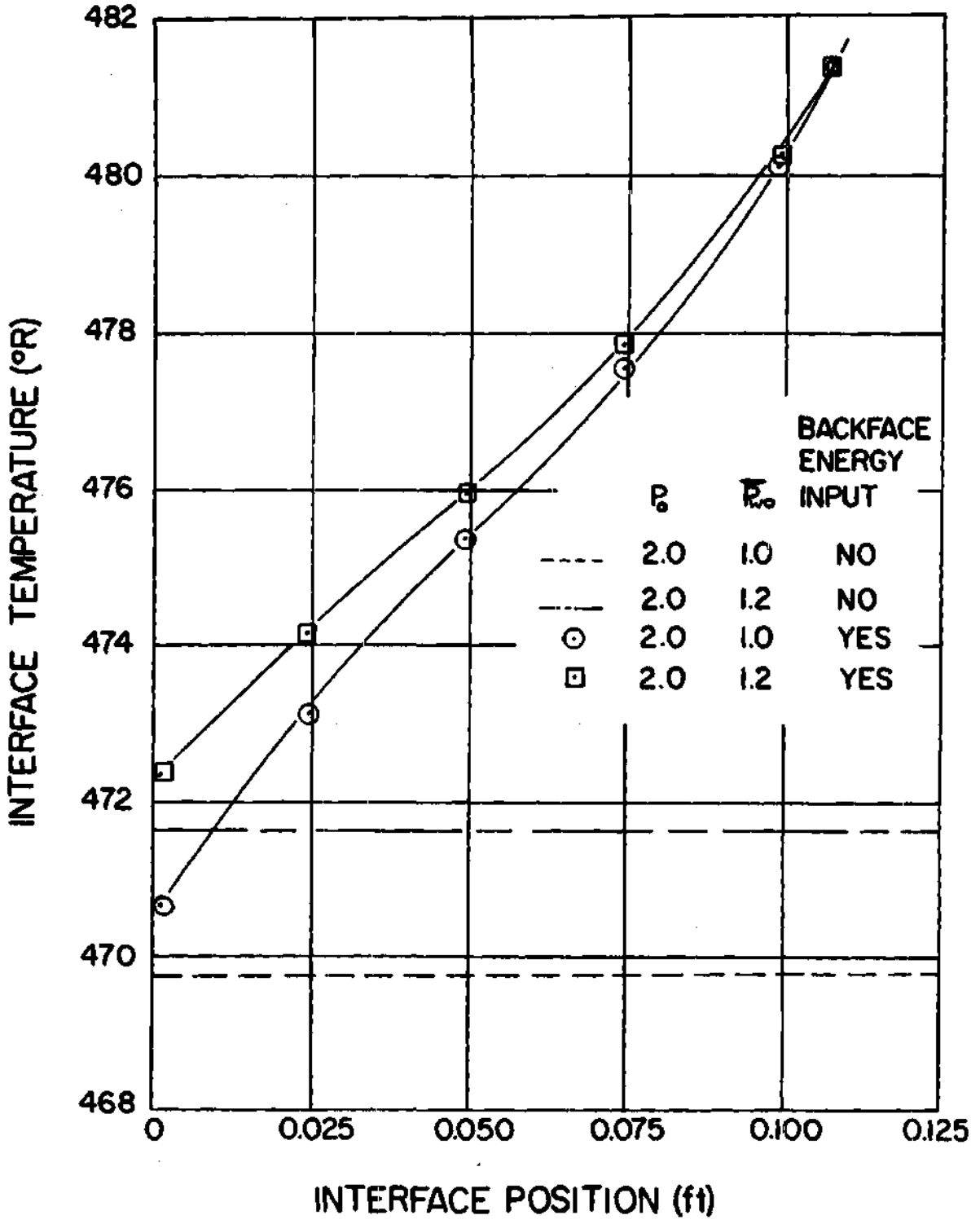

Figure 14. Interface Temperature vs. Interface Position.

back face. In addition, it is seen that the interface temperature increases with the increase of water-vapor concentration in the chamber. An explanation for this result is given in the previous section.

The validity of the assumed interface temperature used as a boundary condition in the calculation of the results for Chapter II was checked by plotting chamber water-vapor concentration versus interface temperature. This plot, Figure 15, is for the following conditions: back face heating, chamber pressure of 2 torr, and interface positions X/L of 0.09 and 0.5. Note that as the chamber water-vapor concentration approaches 1.0 for small values of X/L (for example .09), the interface temperature approaches a value equal to the saturation temperature of meat for the chamber pressure. This corresponds to the assumption in Chapter II. However, at larger values of X/L (for example 0.5) the interface temperature becomes larger than the saturation temperature corresponding to the chamber pressure. Thus, the boundary condition used in Chapter II is valid during the initial stages of drying for high chamber water-vapor concentrations. Therefore, the results are only an approximation to the complete solution as given in Chapter III, but they are easier to apply and give fairly accurate results as can be seen in a perusal of Appendix D.

Relative Contribution of Bulk and Hydrodynamic Flow

There has been considerable discussion concerning the relative contributions of hydrodynamic and diffusional flow in freeze-drying. With the derivation of equation 3.20 and the determination of the effective diffusion coefficient it is possible to quantitatively estimate the relative contribution due to each effect. The differential

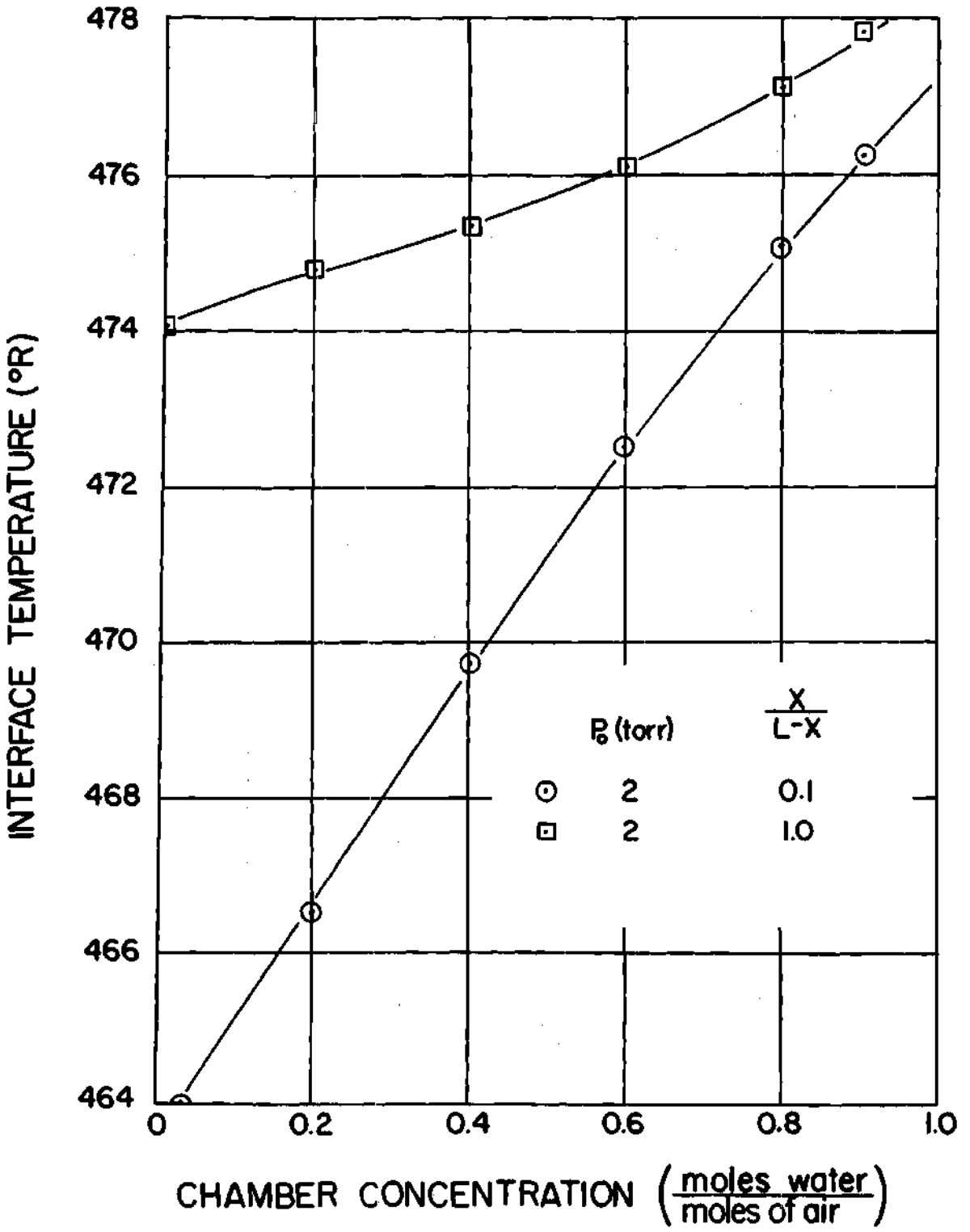

Figure 15. Interface Temperature Versus Chamber Concentration.

form of equation 3.20 assuming ρD_{te} independent of concentration is

$$N_w = - \frac{pD_{te}}{\tilde{R}T} \frac{dy_w}{dx} + N_w y_w \qquad (6.1)$$

Bird, et al (12) point out that the terms on the right hand side of equation 6.1 represent the molar transport of water-vapor due to concentration diffusion and hydrodynamic flow respectively. Substituting equation 3.24 into 6.1, approximating dy_w/dx by $(y_{w0} - y_{wX})/X$ and y_w by $(y_{w0} + y_{wX})/2$ gives

$$N_w = - \frac{pD_{te}}{\tilde{R}T} \frac{y_{w0} - y_{wX}}{X} + \frac{y_{w0} + y_{wX}}{2} \tilde{\varepsilon} \frac{\Delta p}{X} \qquad (6.2)$$

For convenience define

$$\Phi = \frac{\text{Diffusional Transport}}{\text{Hydrodynamic Transport}} \qquad (6.3)$$

Substituting the terms of equation 6.2 representing the diffusional and hydrodynamic transport rates into equation 6.3 and simplifying gives

$$\Phi = \frac{2p\ D_{te}}{\varepsilon \tilde{R}T \Delta p} \left[\frac{y_{wX} - y_{w0}}{y_{wx} + y_{w0}} \right] \qquad (6.4)$$

From equation 6.4 it is seen that increasing concentration gradients will increase the diffusional flux with respect to the hydrodynamic flow while increasing the total pressure gradient has the opposite effect. This result is to be expected when it is recognized that diffusional flow is due to a concentration gradient and hydrodynamic flow is due to a total pressure gradient. To indicate typical values for Φ, the results

of Chapter III were used in conjunction with equation 6.4 in obtaining Figure 16, which is a plot of Φ versus chamber water-vapor concentration for a chamber pressure of 2 torr and a interface position X = .0625 feet. The property values and dimensions for the sample considered are the same as those used in calculating typical results for Chapter III (see page 72).

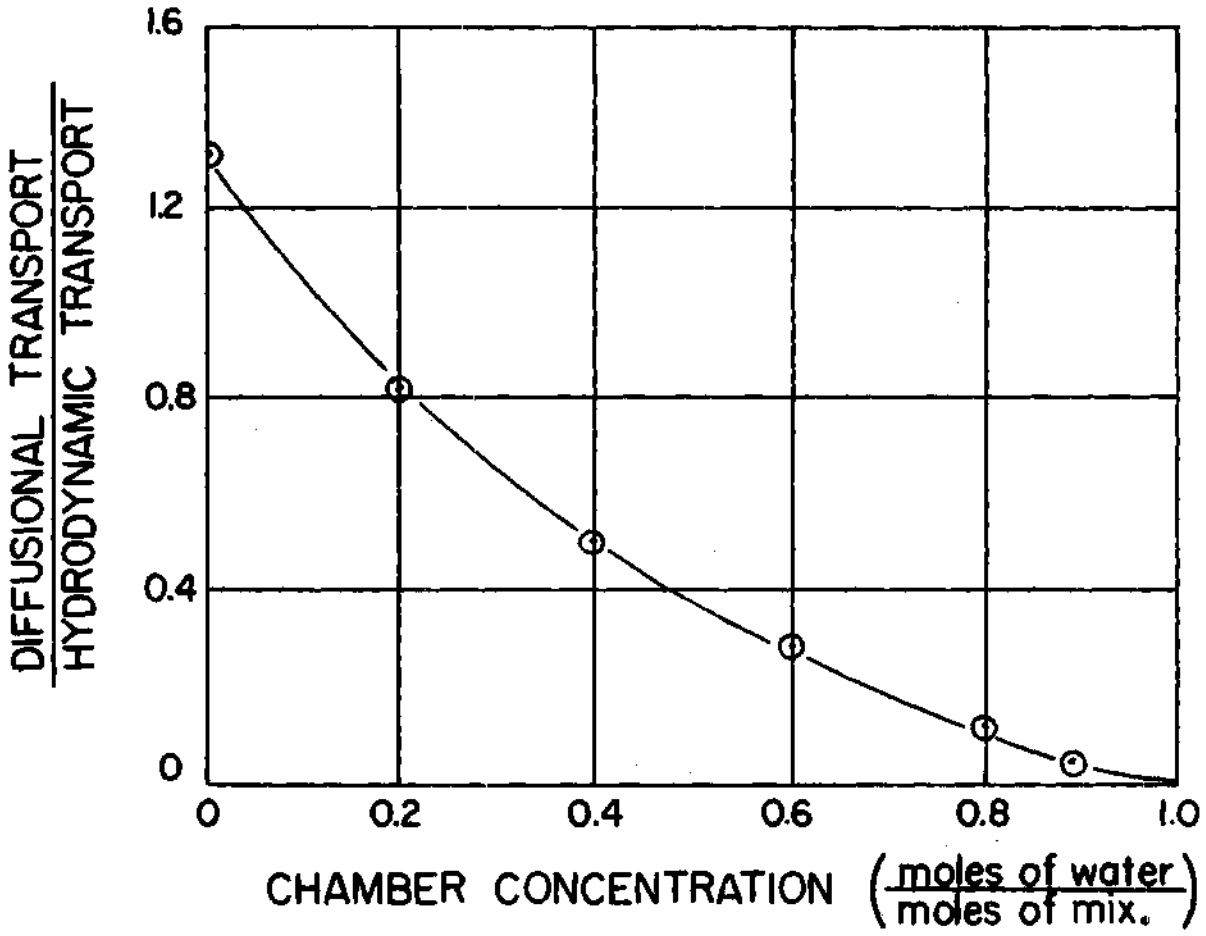

Figure 16. Ratio of Diffusional to Hydrodynamic Transport Versus Chamber Concentration.

CHAPTER VII

CONCLUSIONS

The major conclusions to be drawn from the experimental and theoretical investigation of this work are:

1. The equilibrium vapor pressure of frozen beef is depressed from that of pure ice. In addition, the latent heat of sublimation is greater for frozen beef than pure ice. Both effects are attributable to the dissolved solute species in the meat.

2. The permeability coefficient varies about 10 per cent with different grades, cuts and preparation of beef samples used. In addition, the permeability is thickness dependent possibly due to crimping at the ends of the capillary tubes. The temperature effect on permeability can be accounted for using the procedure outlined beginning page 67.

3. The effective average diffusion coefficient can not be accurately predicted from knowledge of the thermal conductivity as suggested by Harper (17). Equations 3.15 and 3.16 can be used as outlined on page 32 to calculate the effective diffusion coefficient. Equations 3.15 and 3.16 were substantiated by experiment.

4. The thermal transpiration effect results in less than 3 per cent of the total flow and can be neglected for practical calculations.

5. Comparison of the exact and quasi-steady solution of Chapter II for the same boundary conditions show that the quasi-steady solution is sufficiently accurate for practical purposes.

6. The quasi-steady solution given in Chapter II is a relatively good approximation to the more refined solution of Chapter III and is much easier to utilize for practical calculations. However, it does not give a good insight into the mechanisms of heat and mass transport in freeze-drying.

7. The results of Chapter III show the interface temperature is a function of the heat input to the interface from the frozen region (Region II), the chamber total pressure and water-vapor partial pressure, and interface positions. The analytical development of Chapter III allows the determination of the interface temperature from knowledge of the boundary conditions external to the frozen sample.

8. The results of Chapter III show that faster drying is achieved by decreasing the chamber pressure, decreasing the chamber partial pressure, and heating from the back face. The first two methods are not ideal for obtaining faster drying rates since equipment and operation costs rise rapidly with decreased total or partial vapor pressure, the drying rate increases very slowly with decreased pressure (for example see Figure 12), and pressures which are too low can produce temperatures which damage the meat quality (see Reference 3). The third method seems to have tremendous potential in achieving optimum drying conditions as can be seen in Figure 12.

9. Using the equations developed in Chapter III along with equation 6.4 the ratio of mass flux due to diffusional flow to hydrodynamic flow can be calculated. Figure 16 shows typical values of this ratio as a function of chamber concentration.

APPENDIX A

DERIVATION OF ENERGY EQUATION

Model and General Assumptions

For Case 1:

The model considered is shown in Figure 17.

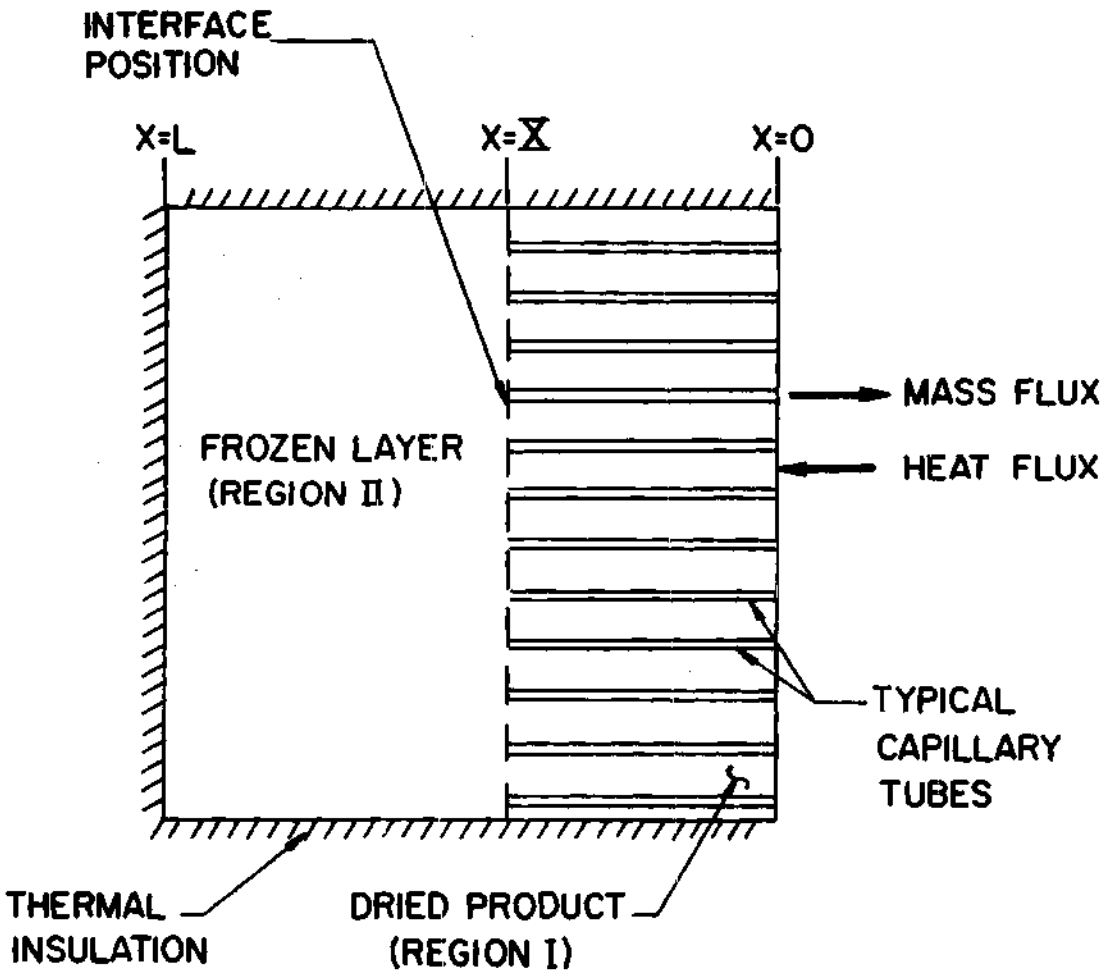

Figure 17. Model of Freeze-Drying Process.

The dried layer is idealized as a bundle of straight circular capillary tubes through which the vapor streams. All heat transfer and fluid flow is assumed to be one dimensional. Due to experimental evidence (11) the local vapor temperature and dried food product temperature are assumed equal. The thermal properties of the meat are assumed constant for each region and, in addition, effective values are defined as follows so that the conventional energy equation can be applied:

$$k_{eI} = \sigma\, k_v + (1 - \sigma)k_D \qquad (A.1)$$

$$\alpha_{eI} = \sigma\, \alpha_v + (1 - \sigma)\alpha_D \qquad (A.2)$$

Derivation of Governing Differential Equation for Case 1

For Region I

Consider the control volume taken from region I and shown in Figure 18.

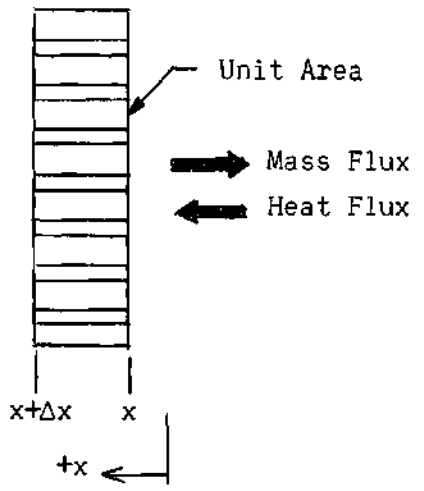

Figure 18. Energy Control Volume for Region I.

The conservation of energy for the control volume is

$$\left[-k_{eI}\left.\frac{\partial T_I}{\partial x}\right|_x + WC_p T_I\Big|_x\right] - \left[-k_{eI}\left.\frac{\partial T_I}{\partial x}\right|_{x+\Delta x} + WC_p T\Big|_{x+\Delta x}\right]$$

$$= \Delta x \frac{k_{eI}}{\alpha_{eI}} \frac{\partial T_I}{\partial t} \qquad (A.3)$$

where the first two terms represent the energy conducted and convected into the control volume, the next two terms represent the energy conducted and convected out of the control volume, and the remaining term represents the increase in energy of the control volume. If equation A.3 is divided through by $A \times k_{eI}$ and multiplied by α_{eI} and the limit taken as $\Delta x \rightarrow 0$, it reduces to

$$\alpha_{eI} \frac{\partial^2 T_I}{\partial x^2} - \frac{WC_p \alpha_{EI}}{k_{eI}} \frac{\partial T_I}{\partial x} = \frac{\partial T_I}{\partial t} \qquad (A.4)$$

The mass flow rate is given by

$$-\rho_i \sigma \frac{dX}{dt}$$

Making this substitution in equation A.4 gives

$$\alpha_{eI} \frac{\partial^2 T_I}{\partial x^2} + \frac{C_p \rho_i \sigma \alpha_{eI}}{k_{eI}} \frac{dX}{dt} \frac{\partial T_I}{\partial x} = \frac{\partial T_I}{\partial t} \qquad (A.5)$$

Calculations by the author based on experimental data show that the convective contribution is less than five per cent of the total heat transfer required. Also it is known that if the convection is neglected the well known Neumann solution is valid which requires that X be proportional

to the square root of time. Therefore, it seems logical to assume for this case in which the convection contribution is small that the interface position is approximately proportional to the square root of time. Writing this assumption in equation form

$$X = b\sqrt{t} \tag{A.6}$$

Also it is convenient to define

$$\nu = \frac{\rho_i \sigma C_p \alpha_{eI}}{k_{eI}} \tag{A.7}$$

Substituting equations A.6 and A.7 into equation A.5 yields

$$\frac{\partial T_I}{\partial t} - \nu \frac{b}{2\sqrt{t}} \frac{\partial T_I}{\partial x} = \alpha_{eI} \frac{\partial^2 T_I}{\partial x^2} \tag{A.8}$$

where it is recognized from equation A.6 that

$$\frac{dX}{dt} = \frac{b}{2\sqrt{t}} \tag{A.9}$$

For Region II

The same energy balance can be applied to this region with the exception that there is no convection term. Then from equation A.8 the governing differential equation for this region can be written down by inspection by deleting the convection contribution. Thus, the equation is

$$\frac{\partial T_{II}}{\partial t} = \alpha_{II} \frac{\partial^2 T_{II}}{\partial x^2} \tag{A.10}$$

Model and General Assumptions

For Case 2

The physical model is again the same as that appearing in Figure 17 with the exception that the face at x = L is not insulated. We again make the same assumptions as for case 1 (see page 9) with the additional assumption that quasi-steady conditions exist. This assumption requires that the space rate of change of properties is much larger than the time rate of change. The boundary conditions for case II (see page 15) require this additional assumption if a closed form solution is desired because of their increased complexity as compared with those for the first model.

Derivation of Governing Differential Equations for Case 2

For Region I

The differential equation will be the same as that for the first case (equation A.5) with the exception that the unsteady term is omitted, i.e.

$$\frac{d^2T_I}{dx^2} + \frac{C_p\rho_I\sigma}{k_{eI}} \frac{dX}{dt} \frac{dT}{dx} = 0 \qquad (A.11)$$

Define

$$\overline{v} = \frac{C_p\rho_i\sigma}{k_{eI}} \qquad (A.12)$$

On substituting this definition into equation A.11 the following result is obtained

$$\frac{d^2T_I}{dx^2} + \bar{v}\,\frac{dX}{dt}\,\frac{dT}{dx} = 0 \qquad \text{(A.13)}$$

For Region II

The differential equation for this region will be the same as for the first Case with the unsteady term omitted, i.e.

$$\frac{\partial^2 T_{II}}{\partial x^2} = 0 \qquad \text{(A.14)}$$

APPENDIX B

ANALYSIS OF HYDRODYNAMIC FLOW IN POROUS MEDIA

Introduction

It is desirable to make an analysis of the mass flow situation in freeze-dried beef in order to determine the relationship between the various flow properties. Although various aspects of flow through porous material have been studied by different investigators, a compilation of their work has not appeared in the literature. The following analysis is chiefly a compilation of the work found in references 9 and 13.

This study presents equations valid for single or multicomponent mixture transport. The model considered is shown in Figure 19.

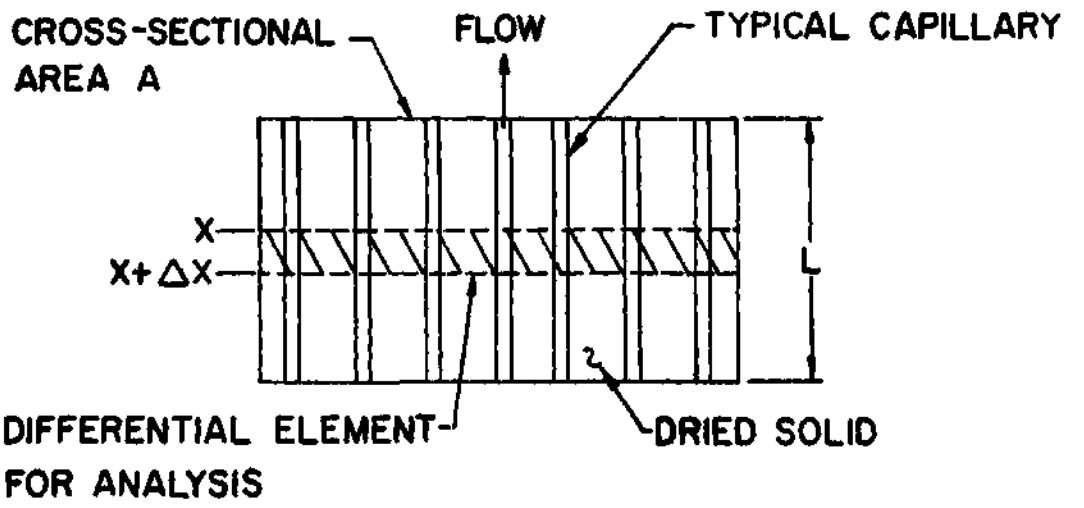

Figure 19. Control Volume for Mass Transport Analysis.

General Conservation of Mass Equation

In order to derive the conservation of mass equation the element shown shaded in Figure 19 will be considered. This equation is

$$\rho Au\Big|_x - \rho Au\Big|_{x+\Delta x} = \frac{\partial}{\partial t}(pA\,\Delta x) \qquad (B.1)$$

where the first term represents mass of vapor in per unit time, the second term represents mass of vapor out per unit time and the last term represents rate of mass accumulation. Substituting the perfect gas equation of state into equation B.1 gives

$$\frac{p}{RT} Au\Big|_x - \frac{p}{RT} Au\Big|_{x+\Delta x} = \frac{\partial}{\partial t}\left(\frac{p}{RT} A\,\Delta x\right) \qquad (B.2)$$

For constant area equation B.2 becomes on taking the limit as $\Delta x \to 0$.

$$\frac{\partial}{\partial x}\left[\frac{p}{RT} u\right] = \frac{\partial}{\partial t}\left[\frac{p}{RT}\right] \qquad (B.3)$$

General Momentum Equation

The method used to analyze the momentum transport in the porous material is to consider the material to be a bundle of capillaries of circular cross sections as illustrated in Figure 18. It will be sufficient to analyze the flow in a single capillary and modify the results for the porous media. An element of gas taken out of the capillary is shown in Figure 20.

From Newton's law for the element shown in Figure 20 the following equation is obtained

$$\Sigma F_x = \frac{\partial}{\partial t} (m_g u) \tag{B.4}$$

where forces are considered positive in the positive x direction and m_g is mass of gas in element. The net forces acting on the element are now substituted into the left side of equation B.4 and the argument of the left side is expanded to yield

$$2\pi r \Delta r\, p\Big|_x - 2\pi r \Delta r\, p\Big|_{x+\Delta x} + 2\pi r \mu \frac{\partial u}{\partial r}\Big|_{r+\Delta r} (\Delta x)$$

$$- 2\pi r \mu \frac{du}{dr}\Big|_r (\Delta x) = \frac{\partial}{\partial \tau}\left[\frac{p}{RT} u\, 2\pi r \Delta r\, \Delta x\right] \tag{B.5}$$

These force terms represent the pressure force at x, the pressure force at $x + \Delta x$, the viscous force on the surface at $r + \Delta r$, and the viscous

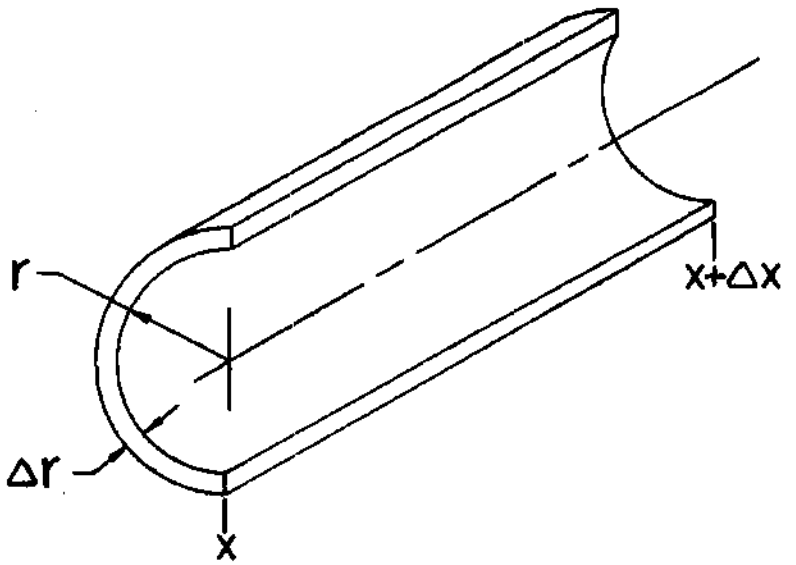

Figure 20. Element of Gas From Capillary.

force on the surface at r respectively. Rearranging and taking the limit of equation B.4 as both $\Delta x \to 0$ & $\Delta r \to 0$ results in the following differential equation.

$$- r \frac{\partial p}{\partial x} + \frac{\partial}{\partial r} \left(r \mu \frac{\partial u}{\partial r} \right) = r \frac{\partial}{\partial t} \left[\frac{p}{RT} u \right] \qquad (B.6)$$

This is the final form of the general momentum equation to be utilized.

Solution of Governing Equations for Transition Flow

Equations B.2 and B.6 will be simplified by assuming quasi-steady flow (i.e. the time derivatives are negligible with respect to the space derivatives). Equation B.3 can then be written as a total differential equation as follows:

$$\frac{d}{dx} \left[\frac{p}{RT} \right] u = 0 \qquad (B.7)$$

In order to obtain a simplified momentum equation, the additional assumptions of constant density and viscosity and fully developed flow are made. With these additional assumptions which have been found valid by preliminary calculations based on expected average values, the following equation is obtained from equation B.6

$$\frac{1}{\mu} \frac{dp}{dx} = \frac{1}{r} \frac{d}{dr} \left(r \frac{du}{dr} \right) \qquad (B.8)$$

Noting that the left side of equation B.8 is a function of x only and the right side a function of r only it is seen that both sides must be equal to the same constant. Therefore

$$\frac{1}{\mu}\frac{dp}{dx} = \frac{1}{r}\frac{d}{dr}\left(r\frac{du}{dr}\right) = C_{13} \tag{B.9}$$

Integrating gives

$$p = \mu C_{12}x + C_{13} \tag{B.10}$$

Applying the boundary conditions that $p = p_o$ at $x = 0$ and $p = p_L$ at $x = L$ to equation B.10 gives

$$C_{12} = \frac{p_L - p_o}{\mu L} = \frac{1}{r}\frac{d}{dr}\left(r\frac{du}{dr}\right) \tag{B.11}$$

Integration of equation B.11 yields on observing that u must be defined at $r = 0$

$$u = \frac{C_{12}}{4}r^2 + C_{14} \tag{B.12}$$

Applying equation B.11 to B.12 gives

$$u = \frac{1}{4}\frac{p_L - p_o}{\mu L}r^2 + C_{14} \tag{B.13}$$

The constant C_{14} will be determined by choosing an appropriate wall boundary condition. For the case under consideration, the mean free path x is approximately equal to the diameter of the tube. This condition results in the so-called "slip flow" in which a velocity exists at the wall. The following definition is made for a force coefficient at the wall

$$C_F = \frac{F_{wall}}{(u_e\ \pi\ 2r_e\ L)} \tag{B.14}$$

where F_{wall} is the viscous force on the wall.

Applying Newton's law to all of the vapor contained in a capillary tube it can be shown that

$$2\pi r\,\Delta r\,p_o - 2\pi r\,\Delta r\,p_L - C_F\,2\pi r\,L u_o + 2\pi r\,L\left(-\mu\,\frac{\partial u}{\partial r}\right)\Big|_{r=r_c} = 0 \quad \text{(B.15)}$$

Taking the limit as $\Delta r \rightarrow 0$ and rearranging gives:

$$u_c = -\frac{\mu}{C_F}\,\frac{du}{dr}\Big|_{r=r_c} \quad \text{(B.16)}$$

Taking the derivative of equation B.13, evaluating at $r = r_c$, and substituting into equation B.16 gives:

$$u_{r=r_c} = -\frac{\mu}{C_F}\,\frac{p_L - p_o}{2\mu L}\,R \quad \text{(B.17)}$$

Thus, the boundary condition at the wall in terms of a force coefficient has been obtained. Substituting equation B.17 into equation B.13 and evaluating at $r = r_c$ gives on rearrangement

$$C_{14} = -\frac{p_L - p_o}{4\mu L}\left[\frac{\mu}{C_F}\,2r_c + r_c^2\right] \quad \text{(B.18)}$$

Substituting equation B.18 into equation B.13 gives the desired expression for the velocity distribution in terms of the force coefficient

$$u = -\frac{p_L - p_o}{4\mu L}\left[\frac{\mu}{C_F}\,2r_c + r_c^2 - r^2\right] \quad \text{(B.19)}$$

To obtain the mass flow rate, it is necessary to integrate the product

of the local velocity given by equation B.19, the differential area, and gas density over the entire cross-sectional area as shown below

$$W = -\int_0^{r_c} 2\pi r\rho \frac{p_L - p_o}{4\mu L}\left[\frac{\mu}{C_F} 2r_c + r_c^2 - r^2\, dr\right] \qquad (B.20)$$

Integrating and evaluating the limits gives

$$W = -\frac{\pi(p_L - p_o)\rho}{8\mu L} r_c^4\left[1 + \frac{\mu}{C_F}\frac{4}{r_c}\right] \qquad (B.21)$$

The ratio μ/C_F is called the coefficient of slip. For diffuse reflections of a Maxwellian gas the coefficient can be determined analytically to be (9)

$$\frac{\mu}{C_F} = \frac{\mu}{p_m}\sqrt{\frac{\pi RT}{2M}}\left(\frac{2-S}{S}\right) \qquad (B.22)$$

Substituting this expression into equation B.21 gives

$$W = -\frac{\pi\rho(p_L - p_o)}{8\mu L} r_c^4\left[1 + \frac{\mu}{p_m}\sqrt{\frac{\pi RT}{2M}}\left(\frac{2-S}{S}\right)\frac{4}{r_c}\right] \qquad (B.23)$$

Equation B.23 is valid for slip flow through a single capillary. Several corrections enumerated below will make equation B.23 valid for use with porous media.

(1) W has units of $ft^3/$(unit area of capillary)(sec) in equation B.23. To get total flow in a unit area of food sample we must multiply by the capillary area divided by the food product surface area. This ratio is defined as the porosity σ.

(2) The vapor actually travels a longer, tortuous path through the food sample so that equation B.23 must be corrected by multiplying the length by the tortuosity factor τ.

(3) In addition, a first order correction for the nonroundness and other irregularities of the capillaries can be made by multiplying equation B.23 by a constant Γ.

Applying the above corrections to equation B.23 gives the following equation valid for slip flow through porous media.

$$W = - \rho\Gamma \frac{\pi(p_L - p_o)}{8\mu L \tau} r_c^4 \sigma \left[1 + \frac{\mu}{p_m}\sqrt{\frac{\pi RT}{2M}} \left(\frac{2 - S}{S}\right) \frac{4}{r_c}\right] \qquad (B.24)$$

Define

$$\Delta p = p_L - p_o \qquad (B.25)$$

$$B_4 = \frac{\Gamma\pi r_c^4 \sigma}{8\tau} \qquad (B.26)$$

$$B_5 = \sqrt{\frac{\pi R T}{2M}} \frac{2 - S}{S} \frac{4}{r_c} \mu \qquad (B.27)$$

Substituting equations B.25 through B.27 into equation B.24 gives

$$W = - \frac{\Delta p}{L} \rho B_4 \left[1 + \frac{B_5}{p_m}\right] \qquad (B.28)$$

Note that B_4 and B_5 are only functions of the porous material, average temperature, and gas flowing and should be constant for a given gas, temperature, and porous sample. Scott (13) points out that equation B.28 fails to correlate experimental data for flow through porous media. The

reason for this failure is attributed to the fact that in the derivation of the slip flow term all of the molecules were assumed to have undergone intermolecular collisions between two successive wall collisions. At r_c/λ approximately equal to 1/2 it seems logical that a fraction of the molecules do not undergo these intermolecular collisions. A modification of equation B.28 is required to take this into account. We assume a certain fraction of the molecules $F(r_c/\lambda)$ do not undergo intermolecular collisions. This fraction to a first approximation is considered to flow as described by Knudsen's equation for molecular streaming. Equation B.28 is assumed to describe properly the remaining fraction of the molecules. With this background equation B.28 can be modified as follows

$$W = \left[1 - F(r_c/\lambda)\right]\left[-\frac{B_4 \Delta p \bar{p}}{\mu L}\left(1 + \frac{B_5}{\bar{p}_m}\right)\right] + B_3 \frac{\Delta p}{L} F(r_c/\lambda) \qquad (B.29)$$

where B_3 is a constant given by kinetic theory (13)

$$B_3 = \frac{16 r_c^3}{3mL}\left(\frac{\pi m}{8KT}\right)^{1/2}$$

By use of kinetic theory assuming diffuse reflections and a long capillary tube it can be shown that the fraction $F(r_c/\lambda)$ is given by (13)

$$F(r_c/\lambda) = \frac{4}{\pi}\int_0^{\pi/2}\int_0^{\pi/2} \sin\theta \cos\theta \exp\left[\left(-\frac{\cos\varphi}{\sin\theta}\right)\frac{2r_c}{\lambda}\right] d\theta d\varphi \qquad (B.30)$$

For small values of r_c/λ such as encountered in this case equation B.30 can be integrated by numerical integration to give

$$F(\bar{r}_c/\lambda) = \exp(-2\bar{r}_c/\lambda) \tag{B.31}$$

Substituting equation B.31 into equation B.29 yields on rearrangement

$$W = -\left[1 - \exp(-2\bar{r}_c/\lambda)\right]\left[\frac{B_4 \Delta p p}{\mu L}\left(1 + \frac{B_5}{p_m}\right)\right] + B_3 \frac{\Delta p}{L} \exp(-2\bar{r}_c/\lambda) \tag{B.32}$$

For continuous flow $\exp(-2\bar{r}_c/\lambda) \rightarrow 0$ and $B_2 \ll p_m$. Therefore for continuous transport

$$-\frac{\mu W L}{\rho \Delta p} = B_4 \tag{B.33}$$

But for continuous flow through a porous material Darcy's law (10) is known to apply

$$W = -\rho \frac{\epsilon_D}{\mu} \frac{\Delta p}{L} \tag{B.34}$$

where ϵ_D is called the permeability. From comparison of equations B.33 and B.34 it is seen that

$$\epsilon_D = B_4 \tag{B.35}$$

Thus, B_4 represents the permeability for continuous transport, i.e. the permeability as defined in Darcy's law. By analogy with Darcy's law for the present case of transition flow, the permeability will be defined by

$$\epsilon(p_m) = -\frac{\mu W L}{\rho \Delta p} \tag{B.36}$$

By comparing equations B.32 and B.36 it is seen that

$$\epsilon(p_m) = + [1 - \exp(-2r_c/\lambda)][B_4(1 + B_5/p_m)] + \frac{\mu B_3}{\rho} \exp(-2r_c/\lambda) \quad (B.37)$$

where the permeability has been symbolized by $\epsilon(p_m)$ to emphasize that it is a function of average pressure whereas ϵ_D was not pressure dependent. Expressing the density by the ideal gas law in equation B.36 gives the final form of the momentum equation for transition flow.

$$W = - \rho \frac{\epsilon(p_m)}{\mu} \frac{\Delta p}{L} \quad (B.38)$$

APPENDIX C

PERMEABILITY DATA

Table 3. Experimental Permeability Data

Method*	p_m(torr)	Δp(torr)	$W_w(\frac{gm}{cm^2\ sec})$	L(cm)	ε'(sq ft)x10^8
2	0.70	0.50	0.13	3.17	2.56
2	0.86	0.38	0.10	3.17	2.01
2	1.62	0.28	0.05	3.17	0.72
2	3.00	0.24	0.03	3.17	0.28
2	3.76	0.19	0.01	3.17	0.17
2	1.78	0.27	0.04	3.17	0.64
2	0.51	0.37	0.08	2.14	1.92
2	1.24	0.55	0.12	3.17	1.19
2	2.00	0.39	0.06	3.17	0.54
2	3.62	0.25	0.04	3.17	0.35
1	0.72	0.43	0.08	3.17	1.76
1	0.73	0.31	0.07	3.17	2.17
1	0.77	0.24	0.06	3.17	2.31
1	0.81	0.18	0.03	3.17	1.57
1	0.46	0.10	0.05	2.54	6.79
1	1.06	0.28	0.06	3.56	1.69
1	0.69	0.15	0.06	1.27	1.53
1	0.86	0.26	0.05	3.42	1.85
1	0.61	0.12	0.04	2.54	2.76
1	0.69	0.31	0.05	2.42	1.18
1	0.93	0.34	0.04	3.05	0.89
1	0.86	0.40	0.06	2.30	0.88
1	0.56	0.04	0.02	2.80	6.20
1	0.62	0.12	0.04	2.21	2.39
2	0.71	0.48	0.09	3.18	1.84

*Method refers to the apparatus used as described and defined in Chapter IV.

Table 3. Experimental Permeability Data (continued)

Method	p_m(torr)	Δp(torr)	W_w($\frac{gm}{cm^2\ sec}$)	L(cm)	ε'(sq ft) x 10^8
2	1.42	0.43	0.08	3.18	0.97
2	1.72	0.36	0.09	3.18	0.96
2	2.83	0.25	0.04	3.18	0.46
2	0.62	0.45	0.04	1.90	0.68
2	4.12	0.24	0.03	1.90	0.14
2	0.53	0.37	0.05	1.90	1.10
2	1.44	0.21	0.05	1.90	0.86
2	0.73	0.43	0.10	3.55	2.37
2	1.75	0.28	0.06	3.55	0.97
2	2.74	0.24	0.04	3.55	0.50
2	2.50	0.13	0.03	1.90	0.41
2	0.51	0.39	0.11	2.20	2.52
2	0.59	0.31	0.07	2.20	1.89
2	0.97	0.20	0.04	2.20	1.08
2	2.37	0.27	0.03	2.20	0.24
2	0.89	0.37	0.08	2.41	1.25
2	1.87	0.25	0.05	2.41	0.59
2	0.60	0.20	0.04	2.20	1.78
2	0.59	0.13	0.04	2.20	2.50
2	0.62	0.12	0.04	2.20	2.38
2	0.62	0.12	0.04	2.54	2.79
2	0.63	0.10	0.03	2.54	2.53
2	0.76	0.24	0.06	3.17	2.37

APPENDIX D

ANALYTICAL RESULTS

The following property values and dimensions were used in the calculation of the succeeding results:

$L = .125$ ft.

$H = 1220$ B/lbm

$C_p = 0.46$ B/lbm °R

$\alpha = 0.06$ ft^2/hr

$k_{II} = 0.06$ B/ft-hr °R

$k_{eI} = 0.026$ for p = 1 torr

$= 0.028$ for p = 2 torr

$= 0.029$ for p = 3 torr

The thermal boundary conditions used were

$T_o = 560$ °R

$T_L = T_X$ for no back face heating

$T_L = 488$ °R for back face heating

T_X = equilibrium temperature of beef for the chamber pressure (cases I and II)

T_X = determined analytically in the results of Chapter III.

Table 4. Computer Results for Case 1 and 2

X/L	Time Required to Reach Interface Position (hrs)								
	Case 1			Case 2. No Back Face Heating			Case 2. Back Face Heating		
	P_o=1 torr	P_o=2 torr	P_o=3 torr	P_o=1 torr	P_o=2 torr	P_o=3 torr	P_o=1 torr	P_o=2 torr	P_o=3 torr
0.05	0.8	0.8	0.8	0.8	0.8	0.8	0.6	0.6	0.7
0.10	2.2	2.3	2.5	2.0	2.1	2.3	1.5	1.7	2.3
0.15	4.7	4.8	5.75	4.5	4.7	5.0	2.8	3.5	5.0
0.20	8.0	8.5	9.0	8.0	8.3	9.1	4.8	5.6	8.8
0.25	12.6	13.2	14.2	12.6	13.0	14.3	6.2	8.1	13.3
0.30	18.2	18.5	20.5	18.2	18.8	20.7	8.0	10.3	18.9
0.35	24.8	25.8	27.8	24.7	25.7	28.0	9.7	13.4	25.1
0.40	32.0	33.0	36.0	32.2	33.4	36.7	11.7	16.1	32.1
0.45	40.2	41.5	46.2	40.7	42.2	46.3	13.3	18.7	39.6
0.50	49.5	51.5	56.5	50.4	52.0	52.3	14.8	21.3	47.8
0.55	59.5	62.5	68.5	60.9	63.1	69.3	16.3	23.7	56.2
0.60	71.0	74.0	81.0	72.5	75.2	82.5	17.7	26.0	64.8
0.65	83.5	86.5	95.5	85.1	88.0	96.3	18.9	28.0	73.6
0.70	96.0	99.5	110.5	98.8	102.2	112.2	20.1	29.9	82.0
0.75	110.5	115.2	127.0	113.3	117.3	128.5	21.5	31.5	90.2
0.80	126.0	131.0	144.0	129.0	133.5	146.7	21.8	32.9	98.0
0.85	142.0	148.0	163.0	145.0	150.7	165.3	22.3	33.9	104.4
0.90	158.0	165.0	179.0	162.0	169.0	186.0	22.8	34.7	109.3
0.95	177.0	184.0	203.0	180.0	188.0	206.7	23.3	35.3	113.2
1.00	196.0	204.0	225.0	200.0	208.0	228.0	24.0	36.0	115.0

Table 5. Computer Results of Chapter III for Back Face Heating

X/L	$p_w = 0.5(p_0)$						$p_w = 0.6(p_0)$					
	p_0 = 1 torr		p_0 = 2 torr		p_0 = 3 torr		p_0 = 1 torr		p_0 = 2 torr		p_0 = 3 torr	
	t*(hrs)	T_X(°R)	t(hrs)	T_X(°R)	t(hrs)	T_X(°R)	t(hrs)	T_X(°R)	t(hrs)	T_X(°R)	t(hrs)	T_X(°R)
0.05	0.5	461.7	0.5	471.2	.6	476.8	.5	462.7	.5	472.7	.6	478.7
0.10	1.5	462.7	1.7	471.9	1.9	477.3	1.5	463.5	1.8	473.2	2.0	479.0
0.15	2.7	463.6	3.4	472.5	3.8	477.7	2.8	464.2	3.5	473.7	4.0	479.3
0.20	4.5	464.4	5.4	473.1	6.2	478.1	4.5	464.9	5.6	474.1	6.6	479.6
0.25	6.2	465.2	7.7	473.7	9.0	478.5	6.3	465.6	8.0	474.6	9.6	479.8
0.30	8.0	465.7	10.7	474.4	12.1	478.9	8.1	466.2	10.5	475.1	12.9	480.1
0.35	9.0	466.5	12.7	474.8	15.4	479.3	10.0	466.7	13.2	476.0	20.3	480.7
0.40	11.7	467.1	15.4	475.4	18.9	479.7	11.9	467.3	16.0	476.0	20.3	480.7
0.45	13.6	467.7	18.1	475.9	22.4	480.1	13.7	467.9	18.7	476.4	24.1	481.1
0.50	15.4	468.3	20.8	476.5	26.1	480.6	15.9	468.4	21.5	476.9	28.1	481.4
0.55	17.1	468.9	23.4	472.0	29.8	481.0	17.2	469.0	24.2	477.4	32.1	481.8
0.60	18.7	469.6	26.0	477.6	33.5	481.5	18.8	469.6	26.9	477.8	36.1	482.1
0.65			28.5	478.2	37.1	482.0			29.4	478.4	40.0	482.5
0.70			30.9	478.8	40.6	482.5			31.8	478.9	43.8	483.0
0.75			33.0	479.4	44.0	483.1			34.0	479.5	47.4	483.5
0.80			35.0	480.1	47.3	483.7			36.0	480.7	50.9	484.0
0.85			36.7	481.0	50.3	484.4					54.1	484.6
0.90					53.0	485.2					56.9	485.4
0.95					55.4	486.3					59.4	486.4

*t refers to time required to reach interface.

Table 6. Computer Results for Chapter III - No Back Face Heating

X/L	Time Required to Reach Interface Position (hrs)					
	$p_w = 0.5(p_o)$			$p_w = 0.6(p_o)$		
	p_o=1 torr	p_o=2 torr	p_o=3 torr	p_o=1 torr	p_o=2 torr	p_o=3 torr
	*T_X=459.6	T_X = 469.8	T_X = 475.8	T_X = 461.1	T_X = 471.7	T_X = 478.0
0.05	0.5	0.5	0.5	0.5	0.5	0.5
0.10	1.9	1.9	2.0	1.9	2.0	2.1
0.15	4.2	4.4	4.5	4.3	4.4	4.6
0.20	6.8	7.7	8.0	7.7	7.9	8.2
0.25	11.7	12.1	12.5	11.9	12.3	12.8
0.30	16.9	17.4	18.0	17.2	17.8	18.5
0.35	23.0	23.7	24.5	23.3	24.2	25.1
0.40	30.1	31.0	32.0	30.5	31.6	32.8
0.45	38.0	39.2	40.5	38.6	40.0	41.5
0.50	47.0	48.4	50.0	47.6	49.4	51.3
0.55	56.8	58.5	60.4	57.7	59.7	62.0
0.60	67.6	69.6	71.9	68.6	71.1	73.8
0.65	79.4	81.7	84.4	80.5	83.4	86.6
0.70	92.1	94.8	97.9	93.4	96.8	100.5
0.75	105.7	108.8	112.4	107.2	111.1	115.3
0.80	120.2	123.8	127.9	122.0	126.4	131.2
0.85	135.7	139.8	144.3	137.7	142.7	148.2
0.90	152.2	156.7	161.8	154.4	160.0	166.1
0.95	169.6	174.6	180.3	172.0	178.3	185.1
1.00	187.9	193.5	199.8	198.6	197.5	205.1

*Values of T_X were obtained from the computer calculations and have units °R.

LITERATURE CITED

1. Harper, J. C. and A. L. Tappel, Advances in Food Research, Vol. VII, Academic Press, New York, 1957, pp. 171-234.

2. Harris, R. J. C., Biological Applications of Freezing and Drying, Academic Press, New York, 1954.

3. Luyet, B. J., "Rehydration of Freeze Dried Beef," American Foundation for Biological Research, Rept. No. 1, Quartermaster Food and Container Institute, Chicago, 1959.

4. Flosdorf, E. W., Freeze-Drying, Reinhold, New York, 1949.

5. Lambert, J. B., Heat and Mass Transfer in Freeze-Drying, Ph. D. Dissertation, University of Wisconsin, 1956.

6. Bannister, J. D., Heat and Mass Transfer Mechanisms in Sublimation Drying, M. S. Thesis, Northwestern University, 1961.

7. Koumoutous, N. G. and J. E. Sunderland, "Freeze Dehydration," Technika Chronika; Athens, Greece, 1963.

8. Kennard, E. H., Kinetic Theory of Gases, McGraw Hill, New York, 1939.

9. Loeb, L. B., The Kinetic Theory of Gases, McGraw Hill, New York, 1934.

10. Carman, P. C., Flow of Gases Through Porous Media, Academic Press, New York, 1956.

11. Schneider, P. J., Conduction Heat Transfer, Addison Wesley, New York, 1956, pp. 218-221.

12. Bird, B. R., Stewart, W. E. and E. N. Lightfoot, "Diffusivity and the Mechanisms of Mass Transport," Transport Phenomena, John Wiley and Sons, New York, 1960, pp. 495-515.

13. Scott, D. S., and F. A. Dullien, "The Flow of Rarified Gases," American Institute of Chemical Engineers Journal, Vol. 8, No. 3, 1962, pp. 293-297.

14. Scott, D. S., and F. A. Dullien, "Diffusion of Ideal Gases in Capillaries and Porous Solids," American Institute of Chemical Engineers Journal, Vol. 8, No. 1, 1962.

15. Harper, J. C., "Transport Properties of Gases in Porous Media at Reduced Pressures with Reference to Freeze-Drying," American Institute of Chemical Engineers Journal, Vol. 8, No. 3, 1962, pp. 298-302.

16. Harper, J. C. and C. O. Chichester, "Micro-Wave Spectra and Physical Characteristics of Fruit and Animal Products Relative to Freeze Dehydration," Final Report, University of California, Davis, Quartermaster Corps Food and Container Institute Contract DA-19-129-qm-1349, 1960.

17. Harper, J. C. and C. O. Chichester, "Improvements in Rates of Freeze-Drying," Vacuum Symposium Transactions, 1963, pp. 47-53.

18. Hardin, T. C., Heat and Mass Transfer Mechanisms in Freeze-Drying, Ph. D. Thesis, Georgia Institute of Technology, Atlanta, 1965.

19. Hill, J.E., Measurement of Thermal Conductivity, Master's thesis (in progress), Georgia Institute of Technology, Atlanta, Georgia.

20. Massey, W.M., Measurement of Thermal Conductivity During Freeze-Drying of Beef, Master's Thesis (in progress), Georgia Institute of Technology, Atlanta, Georgia.

21. Hatcher, J. D., The Use of Gamma Radiation to Measure Moisture Distribution During Drying Processes, Master's Thesis, Georgia Institute of Technology, Atlanta, Georgia, 1964.

22. Widder, D. V., Advanced Calculus, Prentice Hall, Englewood Cliffs, N. J., 1961, p. 44.

23. Knudsen, M., The Kinetic Theory of Gases, Methuen and Co., Ltd., London, 1934.

24. Evans, R. D., Watson, G. M., and E. A. Mason, "Gaseous Diffusion in Porous Media II. Effect of Pressure Gradients," The Journal of Chemical Physics, Vol. 36, No. 7, 1962, pp. 1894-1902, 1962.

25. Present, R. D., Kinetic Theory of Gases, McGraw-Hill, New York, 1958.

26. Chapman, S., and T. G. Cowling, The Mathematical Theory of Non-Uniform Gases, Cambridge University Press, Cambridge, 1961, p. 415.

27. Dyer, D. F., and J. E. Sunderland, "A Standard for Vapor Pressure Measurement at Low Pressures," Vacuum, Vol. 14, 1964, p. 395.

28. Keenan, J. H., and F. G. Keyes, Thermodynamic Properties of Steam, John Wiley and Sons, New York, 1936.

29. Lewis, G. N., and M. Randall, Thermodynamics, McGraw-Hill, New York, 1961, p. 233.

30. Swalin, R. A., Thermodynamics of Solids, John Wiley and Sons, New York, 1962, p. 147.

31. Weast, R. C., Edt., Handbook of Chemistry and Physics, The Chemical Rubber Co., Cleveland, 1964, Sect. F, p. 18.

32. Licht, W., and D. Stechert, "The Variation of Viscosity of Gases and Vapors with Temperature," Journal of Physical Chemistry, Vol. 48, 1944, pp. 23-47.

33. Guthrie, A., Vacuum Technology, John Wiley and Sons, New York, 1965.

34. Miller, H. L., and J. E. Sunderland, "Thermal Conductivity of Beef," Food Technology, Vol. XVII, No. 4, 1963, p. 490-492.

VITA

David F. Dyer was born in Murfreesboro, Tennessee on October 11, 1939. He spent his pre-college years on his parents' farm at Eagleville, Tennessee and was graduated from Eagleville High School in May 1957.

He began his college work in September 1957 at Middle Tennessee State University where he studied until December 1958. During this period he was placed on the Engineering Co-operative program with ARO, Incorporated in Tullahoma, Tennessee. He transferred to the University of Tennessee in March 1959 and received a B.S. degree in Mechanical Engineering in June 1962. Since September 1962 he has been doing graduate work at the Georgia Institute of Technology where he received a M.S. degree in Mechanical Engineering in June 1964.

Mr. Dyer was married in 1963 to the former Angeline B. McKnight and they have no children.